Molecular Biology of the Cell
Vol. 18, 995–1008, March 2007

Function of the *Caenorhabditis elegans* ABC Transporter PGP-2 in the Biogenesis of a Lysosome-related Fat Storage Organelle

Lena K. Schroeder,* Susan Kremer,†‡ Maxwell J. Kramer,†‡ Erin Currie,*† Elizabeth Kwan,† Jennifer L. Watts,§ Andrea L. Lawrenson,* and Greg J. Hermann*†

*Department of Biology and †Program in Biochemistry and Molecular Biology, Lewis and Clark College, Portland, OR 97219; and §Institute of Biological Chemistry, Washington State University, Pullman, WA 99164

Submitted August 7, 2006; Revised December 19, 2006; Accepted December 22, 2006
Monitoring Editor: Sandra Lemmon

Caenorhabditis elegans **gut granules are intestine specific lysosome-related organelles with birefringent and autofluorescent contents. We identified *pgp-2*, which encodes an ABC transporter, in screens for genes required for the proper formation of gut granules. *pgp-2(−)* embryos mislocalize birefringent material into the intestinal lumen and are lacking in acidified intestinal V-ATPase–containing compartments. Adults without *pgp-2(+)* function similarly lack organelles with gut granule characteristics. These cellular phenotypes indicate that *pgp-2(−)* animals are defective in gut granule biogenesis. Double mutant analysis suggests that *pgp-2(+)* functions in parallel with the AP-3 adaptor complex during gut granule formation. We find that *pgp-2* is expressed in the intestine where it functions in gut granule biogenesis and that PGP-2 localizes to the gut granule membrane. These results support a direct role of an ABC transporter in regulating lysosome biogenesis. Previously, *pgp-2(+)* activity has been shown to be necessary for the accumulation of Nile Red–stained fat in *C. elegans*. We show that gut granules are sites of fat storage in *C. elegans* embryos and adults. Notably, levels of triacylglycerides are relatively normal in animals defective in the formation of gut granules. Our results provide an explanation for the loss of Nile Red–stained fat in *pgp-2(−)* animals as well as insight into the specialized function of this lysosome-related organelle.**

INTRODUCTION

Lysosomes are membrane bound terminal endocytic compartments characterized by an acidic luminal pH and the activity of acid hydrolases (Kornfeld and Mellman, 1989). Specialized, cell type–specific compartments with lysosomal characteristics comprise a functionally diverse group of compartments known as lysosome-related organelles (Dell'Angelica *et al.*, 2000). Lysosome-related organelle functions include the formation and storage of pigment (mammalian melanosomes and *Drosophila* pigment granules; Spritz, 1999; Raposo and Marks, 2002), the regulation of platelet aggregation (platelet dense granules; King and Reed, 2002), and the biogenesis of lung surfactant (lamellar bodies; Weaver *et al.*, 2002).

The human diseases Hermansky-Pudlak, Chediak-Higashi, and Griscelli syndromes result from dysfunctional lysosome-related organelles (Stinchcombe *et al.*, 2004). Hermansky-Pudlak syndrome (HPS) is associated with the abnormal biogenesis of lysosome-related organelles including melanosomes and platelet-dense granules, which is manifested in partial albinism and impaired blood clotting (Huizing *et al.*, 2002; Li *et al.*, 2004). Mutations in eight different human genes are known to cause HPS, and at least seven additional genes are associated with HPS-like phenotypes in rodents (Wei, 2006). HPS genes encode Rab38 and subunits of the AP-3, HOPS, and BLOC-1, -2, and -3 complexes (Dell'Angelica, 2004; Di Pietro and Dell'Angelica, 2005). These proteins function in the sorting and transport of proteins to lysosomes and lysosome-related organelles.

The intestinal cells of the nematode *Caenorhabditis elegans* contain gut granules, cell type–specific compartments that have been proposed to be lysosome-related organelles (Clokey and Jacobson, 1986; Hermann *et al.*, 2005). Gut granules are acidified (Clokey and Jacobson, 1986), contain the vacuolar H^+-ATPase (V-ATPase; Hermann *et al.*, 2005), and act as terminal endocytic compartments (Clokey and Jacobson, 1986; Bossinger and Schierenberg, 1996). Gut granules are distinguished from other lysosomes in *C. elegans* by their birefringent (Laufer *et al.*, 1980) and autofluorescent (Babu, 1974) contents. The biogenesis of gut granules requires *C. elegans* genes encoding homologues of Rab38 and subunits of the AP-3 and HOPS complexes (Hermann *et al.*, 2005). Animals with mutations in these genes show a Glo (gut granule loss) phenotype characterized by loss and/or mislocalization of birefringent material into the embryonic intestinal lumen and/or the loss of adult autofluorescent gut granules.

Disrupting the function of the ABC transporter PGP-2 results in the loss of acidified compartments (Nunes *et al.*, 2005) and fat (Ashrafi *et al.*, 2003; Nunes *et al.*, 2005) in adult *C. elegans* intestinal cells. The function of *pgp-2* in gut granule biogenesis and whether this might explain defects in fat storage exhibited by *pgp-2(−)* animals has not been investigated. In screens for Glo mutants we identified a gene *glo-5*

This article was published online ahead of print in *MBC in Press* (http://www.molbiolcell.org/cgi/doi/10.1091/mbc.E06–08–0685) on January 3, 2007.

‡ These authors contributed equally to this work.

Address correspondence to: Greg J. Hermann (hermann@lclark.edu).

that we show is identical to *pgp-2*. Here we show that *pgp-2* functions directly in gut granule biogenesis, likely in parallel to AP-3, and that gut granules are sites of fat storage in *C. elegans*.

MATERIALS AND METHODS

Strains, Alleles, and Genetics

N2 was used as the wild-type strain. All strains were grown at 22°C and cultured as described (Brenner, 1974). References for mutant alleles are available at www.wormbase.org and are listed by chromosome: linkage group I (LGI): *apt-6(ok429)*, *dpy-5(e61)*, *pgp-2(gk114)*, *pgp-2(kx34)*, *pgp-2(kx48)*, *pgp-2(kx55)*, *pgp-2(kx67)*; LGII: *rrf-3(pk1426)*; LGV: *glo-4(ok623)*; LGX: *apt-7(tm920)*, *glo-1(zu437)*; LG unknown: *bIs33*[*rme-8::gfp*] (Zhang *et al.*, 2001), *pwIs50*[*lmp-1::gfp*] (Treusch *et al.*, 2004), *pwIs87*[*vha-6::rme-1::gfp*] (Hermann *et al.*, 2005), *pwIs72*[*vha-6::rab-5::gfp*] (Hermann *et al.*, 2005); extrachromosomal: *kxEx9*[*glo-1::gfp*] (Hermann *et al.*, 2005), *kxEx41*[*glo-3::gfp*] (Rabbitts and Hermann, unpublished results).

glo-5 alleles were isolated following ethylmethane sulfonate or ethyl nitroso urea-mutagenesis using the method described by Hermann *et al.* (2005). Single nucleotide polymorphism mapping with CB4856 (Davis *et al.*, 2005) placed *kx34*, *kx48*, and *kx67* on LGI between −6 and +5. *kx48* and *kx55* mapped to the *dpy-5 unc-13* genetic interval. Standard genetic tests placed *kx34*, *kx48*, *kx55*, and *kx67* into the *glo-5* complementation group. The Glo phenotypes of all *glo-5* alleles were found to be recessive and expressed zygotically. *kx48* was backcrossed two to five times to N2 and *kx55* was backcrossed two times to N2 before being used for phenotypic studies.

Double mutants were constructed by mating unmarked Glo mutants into *dpy-5(e61)* marked *kx48* or *kx55* mutants to generate transheterozygotes. We isolated Glo non-Dpy adult progeny from the transheterozygotes. Resulting homozygous double mutants were identified by their Dpy phenotype. In all cases at least two independently generated double mutant lines were analyzed and found to exhibit the same phenotype. The linked *dpy-5(e61)* mutation did not alter the Glo phenotypes.

RNA interference (RNAi) using clones from a genomic library (Kamath *et al.*, 2003) was carried out as described in the RNAi-sensitive *rrf-3(pk1426)* background (Simmer *et al.*, 2002).

Microscopy

A Zeiss Axioskop II plus microscope (Thornwood, NY) equipped with DIC, polarization, and fluorescence optics was used for all microscopic analysis. Images were captured with an Insight Spot QE 4.1 camera (Diagnostic Instruments, Sterling Heights, MI). Pretzel stages embryos were placed on slides with excess *Escherichia coli* or briefly chilled to 4°C to induce a paralyzed state before imaging. Larvae and adults were immobilized by mounting in 1× M9 containing 10 mM levamisole. Images used for phenotypic comparisons were always captured at the same exposure times, and brightness and contrast were adjusted identically. Birefringent intestinal material was visualized using polarization optics. Zeiss 9 (Ex:BP450–490; EmLP515) and Zeiss 15 (Ex: BP586/12; Em:LP590) filters were used to visualize autofluorescence. A custom (Ex:BP480/20; Em:BP530/20) filter was used to analyze the colocalization of green fluorescent protein (GFP) signals and birefringent material in living embryos. Staining of adult gut granules with Lysotracker Red (Molecular Probes, Eugene, OR) and embryonic and adult gut granules with acridine orange (Sigma, St. Louis, MO) were performed as described (Hermann *et al.*, 2005). The staining of all lysosomal dyes was analyzed using a Zeiss 15 fluorescence filter set. Endocytosis was monitored by staining with tetramethylrhodamine B isothiocyanate (TRITC)-BSA (Sigma) using the procedure described by Hermann *et al.*, 2005. Fat stores were stained by growing embryo/L1 stage animals to adulthood on seeded nematode growth media (NGM) plates to which Nile Red (Molecular Probes, Eugene, OR) had been added to a final concentration of approximately 50 ng/ml (Ashrafi *et al.*, 2003) or BODIPY 493/503 (Molecular Probes) had been added to a final concentration of ~0.5 ng/ml. Adults and their progeny stained by Nile Red or BODIPY 493/503 were removed from plates and immediately scored. Zeiss 15 and a custom (Ex:BP480/20; Em:BP530/20) filter were used to analyze the colocalization of Nile Red with autofluorescence and GLO-1::GFP. All analysis of GFP in living embryos was carried out using a custom (Ex:BP480/20; Em: BP530/20) filter. Embryos were fixed and stained with mouse 3E6 anti-GFP (Qbiogene, Carlsbad, CA) and affinity-purified rabbit anti-FUS-1 (Kontani *et al.*, 2005), anti-VHA-11 (Oka and Futai, 2000), anti-VPS-27 (Roudier *et al.*, 2005), and anti-PGP-2 (this work) antisera as described (Leung *et al.*, 1999).

Lipid Analysis

Embryos were isolated from adult worms and grown at 22°C on NGM plates with an excess of food until the majority of the population reached young adulthood, indicated by the presence of 1–3 embryos in the uterus. Worms were washed off the plates with 1× M9 and rinsed four times with 1× M9 by letting the worms settle and discarding the supernatant. After the rinses, the worms were spun down in a microfuge tube and as much of the 1× M9 as possible was removed from the final pellet (>400 mg), which was immediately flash-frozen in liquid N_2 and stored at −70°C. Total lipids were extracted from worm pellets, separated using thin-layer chromatography (TLC), and quantified using gas chromatography as described (Brock *et al.*, 2006).

Cloning glo-5

glo-5 mapped to the *dpy-5 unc-13* interval of LGI. The Glo phenotypes of candidate genes located in this interval were assessed using existing mutants or with RNAi. *pgp-2(gk114)* embryos and adults exhibited a Glo phenotype. *pgp-2(RNAi)* in the *rrf-3(pk1246)* background exhibited a strong adult and a weak embryonic Glo phenotype. Three of four stable transmitting *glo-5(kx48)* lines injected with cosmid C34G6 at 10 ng/μl and the coinjection marker pRF4[Rol-6^D] at 100 ng/μl were GLO(+). A 17.3-kb fragment extending from 7.6 kb upstream to 625 base pairs downstream of the *pgp-2* coding sequence was PCR amplified using C34G6 as a template with primers P442 5′CGGATGAGAAGGGAGGGATCTTAGAAG3′ and P460 5′TCGTCGATGAAAACAATGTTACCTTCG3′. All PCR reactions used in these studies utilized Phusion high fidelity DNA polymerase (New England Biolabs, Beverly, MA). The PCR product was coinjected at 10 ng/μl with pRF4[Rol-6^D] at 100 ng/μl. Four of four independently derived transmitting lines were GLO(+). The sequence of mutant alleles was obtained by PCR amplifying the *pgp-2* coding sequences from *glo-5(−)* mutants. Amplifications and DNA sequencing (OHSU Core Facility) were performed in duplicate. The *pgp-2* cDNA was amplified from total RNA isolated using Trizol/chloroform extraction. cDNA was generated using d(T)20 and random hexamers with Superscript III (Invitrogen, Carlsbad, CA). An SL1 primer and a primer specific for the 3′ end of *pgp-2* were used to amplify the full-length cDNA which was sequenced and found to contain an alternative exon 1 (GenBank accession no. EF205592) when compared with the *pgp-2* cDNA predicted by Genefinder (Wormbase160).

Generation of pgp-2::gfp, PGP-2::GFP, and PGP-2 ATPase Mutants

The transcriptional reporter *pgp-2::gfp* was constructed using PCR fusion (Hobert, 2002). A 7.6-kb sequence 5′ of the new predicted translational start of *pgp-2* was amplified using P441 5′CTGTTCGCCAAGCACCCTTCTGAAAAG3′ and P485 5′CAGTGAAAAGTTCTTCTCCTTTACTCATTGAAATGAAGATCTGAACAGAAAAG3′. GFP-NLS was amplified from pPD95.67 using P269 5′ATGAGTAAAGGAGAAGAACTTTTCACTG3′ and P266 5′AAGGGCCCGTACGGCCGACTAGTAGG3′. These two PCR products were fused using P442 and P267 5′GGAAACAGTTATGTTTGGTATATTGGG3′ as described (Hobert, 2002). The resulting *pgp-2::gfp* product was coinjected at 5 ng/μl with pRF4[Rol-6^D] at 100 ng/μl into wild type. *kxEx74*[*pgp-2::gfp;Rol-6^D*] was used for the analysis in this article, and two other independently derived lines showed the same GFP expression pattern.

The translational reporter PGP-2::GFP was constructed by amplifying the full-length *pgp-2* cDNA with P453 5′GGGGACAACTTTGTACAAGAAAGTGTATTGACTTTCGACAATCCTCTGCG3′ and P482 5′GGGGACAACTTTGTACAAAAAAGTTGTGGGAAAAGACACGGAGAAAACTCC3′ and Gateway (Invitrogen) cloning the resulting product using a BP reaction into pDONR221. All transformations of plasmids containing *pgp-2* were carried out using CopyCutter EPI400 (Epicenter, Madison, WI) *E. coli*. The resulting pLKS2 plasmid was fully sequenced to ensure a lack of PCR-generated mutations. *pgp-2* was Gateway cloned using an LR reaction into a VHA-6(promoter)::GFP::GTWYB(EcoRI) vector (Chen *et al.*, 2006). The resulting plasmid pLKS4 contains an N-terminal fusion of *gfp* to *pgp-2* whose expression is regulated by the *vha-6* promoter. The addition of 26 C-terminal amino acids derived from flanking 3′ vector sequences disrupted the function of PGP-2::GFP (not shown). To generate a rescuing PGP-2::GFP construct, PCR fusion was used to introduce a stop codon and the *unc-54* 3′ untranslated region (UTR) at the end of the *pgp-2* coding sequence. *vha-6(promoter)::gfp::pgp-2* was amplified from pLKS4 using P504 5′AAATGAAATAAGCTTGCATGCCTGCAG3′ and P506 5′CCGGCGCTCAGTTGGAATTCTACGATTATTGACTTTCGACAATCCTCTGCG3′ and the *unc-54* 3′ UTR was amplified from pPD95.75 using P507 5′TCGTAGAATTCCAACTGAGCGCCGG3′ and P266. The resulting *vha-6(promoter)::gfp::pgp-2::unc-54* 3′ UTR product was coinjected at 5 ng/μl with pRF4[Rol-6^D] at 100 ng/μl into *pgp-2(kx48)* and wild type. *pgp-2(kx48); kxEx93*[*PGP-2::GFP;Rol-6^D*] was used for the analysis presented in this article, and 13 other independently derived lines showed the same GFP expression pattern. Eleven of fourteen lines were GLO(+). *pgp-2(kx48); kxEx93*[*PGP-2::GFP;Rol-6^D*] showed wild-type patterns of Nile Red–stained fat and acridine orange–stained acidified compartments and was used to determine the cellular localization of PGP-2::GFP in adults. *kxEx98*[*PGP-2::GFP;Rol-6^D*] was used to determine the cellular localization of PGP-2::GFP in embryos.

To express PGP-2::GFP under the control of *unc-119* regulatory sequences (Maduro and Pilgrim, 1995), we performed a triple PCR fusion. The *vha-6(promoter)::gfp::pgp-2* sequence was amplified with P504 and P506 from pLKS4 and the *unc-54* 3′UTR was amplified from pPD95.75 with P507 and P266. The resulting fragments were fused using P269 and P266. *gfp::pgp-2::unc-54* 3′UTR was fused with the *unc-119* promoter amplified from genomic DNA with P495 5′TTTTCCCTTTCCCTCTTGGGGAAAACGGG3′ and P496 5′CAGTGAAAAGTTCTTCTCCTTTACTCATATATGCTGTTGTAGCTGAAAATTTTGGGG3′ using P508 5′TCGAAGACAAACTTTTCAAAAAATTG3′ and P267. The resulting *unc-119(promoter)::gfp::pgp-2::unc-54* 3′ UTR product was coinjected at 5 ng/μl with pRF4[Rol-6^D] at 100 ng/μl into *pgp-2(kx48)*. *unc-*

119(promoter)::gfp::pgp-2::unc-54 3′ UTR was expressed throughout the nervous system and did not rescue the loss of adult autofluorescence in 3/3 independently derived lines. *pgp-2(kx48); kxEx100*[*unc-119::PGP-2::GFP;Rol-6^D*] was scored for rescue of adult Nile Red–stained fat and acridine orange–stained acidified compartments.

To alter the ATPase domains of PGP-2, site-directed mutagenesis with Quickchange II (Stratagene, La Jolla, CA) with primers P501 5′GGTCGGTTCAAGTGGTTGTGGAAGATCAACAATTG3′ and P501R 5′CAATTGTTGATCTTCCACAACCACTTGAACCGACC3′ were used to change Lys_{440} to Arg and primers P502 5′GGCACTCAGGATGTGGAAGATCTACAATTATGGG3′ and P502R 5′CCCATAATTGTAGATCTTCCACATCCTGAGTGCC3′ were used to change Lys_{1069} to Arg in plasmid pLKS4 to generate two plasmids pSK7 and pSK8, respectively. The P502 and P502R primers were used to change Lys_{1069} to Arg in pSK7 resulting in the double ATPase mutant (pSK9). The coding sequences of *pgp-2* and *gfp* were fully sequenced to verify no other mutations were introduced during mutagenesis. We performed the same PCR fusion steps as used in the generation of *vha-6(promoter)::gfp::pgp-2::unc-54* 3′ UTR to construct *vha-6(promoter)::gfp::pgp-2(K440R)::unc-54* 3′ UTR, *vha-6(promoter)::gfp::pgp-2(K1069R)::unc-54* 3′ UTR, and *vha-6(promoter)::gfp::pgp-2(K440R; K1069R)::unc-54* 3′ UTR. These were each coinjected at 1–5 ng/μl with pRF4 [Rol-6^D] at 100 ng/μl into *pgp-2(kx48)* and wild type. The resulting transmitting lines with comparable levels of PGP-2::GFP expression were characterized. *pgp-2(kx48); kxEx102* [*PGP-2(K440R)::GFP;Rol-6^D*] was used for the analysis presented in this article, and 2/2 other independently derived lines showed similar partial rescue of autofluorescence. *pgp-2(kx48); kxEx102* was scored for rescue of Nile Red–stained fat and acridine orange–stained acidified compartments and *pgp-2(+); kxEx104* [*PGP-2(K440R)::GFP;Rol-6^D*] was used to determine the cellular localization of PGP-2(K440R)::GFP in adults. *pgp-2(kx48); kxEx103* [*PGP-2(K1069R)::GFP;Rol-6^D*] was used for the analysis presented in this article, and 3/3 other independently derived lines showed similar partial rescue of autofluorescence. *pgp-2(kx48); kxEx103* was scored for rescue of Nile Red–stained fat and acridine orange–stained acidified compartments, and *pgp-2(+); kxEx105* [*PGP-2(K1069R)::GFP;Rol-6^D*] was used to determine the cellular localization of PGP-2(K1069R)::GFP in adults. *pgp-2(kx48); kxEx115* [*PGP-2(K440R; K1069R)::GFP;Rol-6^D*] was used for the analysis presented in this article, and one other independently derived lines showed similar partial rescue of autofluorescence and Nile Red staining. *pgp-2(kx48); kxEx115* was scored for rescue of Nile Red–stained fat and acridine orange–stained acidified compartments, and *pgp-2(+); kxEx117* [*PGP-2(K440R; K1069R)::GFP;Rol-6^D*] was used to determine the cellular localization of PGP-2(K440R; K1069R)::GFP in adults.

PGP-2 Antibodies

Affinity-purified antibodies recognizing PGP-2 were generated by Bethyl Laboratories (Montgomery, TX). Peptides corresponding to amino 1MGKDTEKTPLLLKS-cys14 and carboxy 1259cys-YQKFsETQRIVESQ1272 (C1263S) terminal PGP-2 sequences were synthesized, coupled to KLH, and used for immunization. Agarose-linked peptides were used to affinity-purify antibodies. The specificity of each antisera was confirmed using *pgp-2(kx48)* Arg466-stop embryos. The anti-carboxy terminal PGP-2 antisera was used in the studies presented here; however, identical results were observed using the anti-amino terminal PGP-2 antisera.

RESULTS

Identification of glo-5 as pgp-2

In genetic screens for Glo mutants we identified four alleles of a gene we named *glo-5* (see *Materials and Methods*) that exhibited mislocalization of birefringent material into the embryonic intestinal lumen and contained greatly reduced numbers of birefringent and autofluorescent gut granules. We mapped *glo-5* to a 2.07 map unit region of the genome defined by *dpy-5* and *unc-13*. Using a candidate gene approach, we found that *pgp-2(gk114)* and *pgp-2(RNAi)* animals exhibited a Glo phenotype very similar to *glo-5(kx48)* and *glo-5(kx55)* (Table 1). *pgp-2(gk114)* did not complement the Glo phenotypes of *glo-5(kx34)*, *glo-5(kx48)*, or *glo-5(kx55)*. The genomic cosmid C34G6, containing *pgp-2*, and the *pgp-2* coding sequence amplified from wild type, rescued the Glo phenotype of *glo-5(kx48)* (not shown). DNA sequencing showed that each *glo-5* allele, *kx34*, *kx48*, *kx55*, and *kx67*, had a mutation that altered the predicted coding sequence of *pgp-2* (Figure 1A). We isolated and sequenced *pgp-2* cDNAs and found that the predicted coding sequence for *pgp-2* (Wormbase WS160) was in error; the *pgp-2* mRNA encodes an alternate first exon. The full-length *pgp-2* cDNA rescued the Glo phenotype of *glo-5(kx48)* (see Figure 9H). Given these data, we have renamed *glo-5* as *pgp-2*.

pgp-2 encodes a member of the ABCB subfamily of ABC transporters. The best understood ABCB protein is human P-glycoprotein (Pgp) encoded by the MDR1 gene, which plays a significant role in tumor cell resistance to anticancer agents (Sheps *et al.*, 2004). Similar to other ABCB proteins, PGP-2 is predicted to have a domain structure composed of six transmembrane (TM)-spanning domains preceding a cytoplasmic ATPase domain, followed by another 6-TM-spanning domains preceding a cytoplasmic ATPase domain (Holland *et al.*, 2003; Figure 1B). Most ABC transporters function by coupling ATP hydrolysis to active transport (Jones and George, 2004). The *kx48* allele is predicted to truncate the PGP-2 protein between the Walker A and Walker B motifs in the first ATPase domain (Figure 1B) and results in the lack of detectable PGP-2 expression in embryos (see Figure 8D) and adults (not shown), thus the *kx48* mutation is likely to severely disrupt *pgp-2* function and represent a null allele.

pgp-2 Functions in Gut Granule Biogenesis

Wild-type gut granules contain birefringent material from the bean (Hermann *et al.*, 2005) through pretzel-stages of embryogenesis (Table 1 and Figure 2B). In *C. elegans*, the stages of embryogenesis are named after the morphology of the embryo (Sulston *et al.*, 1983). Body elongation begins at the bean stage, transforming the ball of embryonic cells into a worm that appears pretzel-like in the eggshell. Between bean and pretzel, the stages of development are described by the length of the embryo relative to the length of the eggshell. Bean-to-hatching stage *pgp-2(−)* embryos contained substantially reduced numbers of birefringent granules within their intestinal cells when compared with wild type (Table 1 and Figure 2, D and F). During the late pretzel stage, *pgp-2(−)* embryos mislocalized birefringent material into the intestinal lumen (Figure 2F). This material was defecated upon hatching (data not shown).

We determined whether *pgp-2* was necessary for the biogenesis of gut granules, or just for the formation and localization of their birefringent contents. In wild-type embryos, gut granules are acidified and are characterized by the presence of the vacuolar H^+-ATPase (V-ATPase) and the Rab GTPase GLO-1 (Hermann *et al.*, 2005). In comparison to wild type (Figure 3, A and U), intestinal cells in *pgp-2(kx48)* 1.5-fold (Figure 3B) and pretzel-stage (Figure 3W) embryos contained few acidic compartments stained by the lysosomal dye acridine orange. FUS-1 is an integral membrane subunit of the V-ATPase (Kontani *et al.*, 2005) that localizes to gut granules in wild-type embryos (Hermann *et al.*, 2005; Figure 3C). FUS-1 staining was not detectible in *pgp-2(kx48)* embryonic intestinal cells (Figure 3D). Similar results were seen when the localization of a peripheral membrane–associated subunit of the V-ATPase, VHA-11 (Oka and Futai, 2000), was analyzed (Figure 3F). GLO-1 is a gut granule membrane-associated Rab GTPase, homologous to mammalian Rab38 and *Drosophila melanogaster* RabRP1/lightoid (Hermann *et al.*, 2005). GLO-1::GFP localized to gut granules in wild-type embryos (Hermann *et al.*, 2005; Figure 3G). In *pgp-2(kx48)* embryonic intestinal cells, GLO-1::GFP was observed as small puncta that did not resemble gut granules in their morphology, number, or distribution (Figure 3H). We conclude that gut granule formation is severely disrupted in *pgp-2(kx48)* embryos and that the mislocalization of birefringent material into the intestinal lumen is likely a consequence of altered gut granule biogenesis.

To better understand the role of *pgp-2* in gut granule biogenesis, we investigated the subcellular localization of

Table 1. Birefringent and autofluorescent gut granules

Genotype	% of embryos with the specified number of birefringent granules in intestinal cells			% of L4/young adults with the specified number of autofluorescent organelles in intestinal cells		
	None	1–100	>100[a]	0–10	11–100	>100[b]
Wild type	0	0	100 (>200)	0	0	100 (>200)
ABCB transporters						
pgp-1(pk17)	0	0	100 (40)	0	0	100 (20)
pgp-2(kx48)	0	96	4 (83)	0	100	0 (25)
pgp-2(kx55)	0	92	8 (75)	0	100	0 (25)
pgp-2(gk114)	0	94	6 (68)	0	100	0 (20)
pgp-2(RNAi)[c]	0	100	0 (62)	0	100	0 (23)
pgp-3(pk18)	0	0	100 (34)	0	0	100 (20)
pgp-4(gk17)	5	0	95 (42)	0	0	100 (20)
pgp-5(ok663)	0	0	100 (45)	0	0	100 (20)
pgp-6(ok994)	0	0	100 (40)	0	0	100 (20)
pgp-7(ok528)[d]	0	0	100 (200)	0	0	100 (24)
pgp-8(RNAi)[c]	0	0	100 (40)	0	0	100 (24)
pgp-9(RNAi)[c]	0	0	100 (50)	0	0	100 (25)
pgp-10(ok991)	0	2	98 (47)	0	0	100 (25)
pgp-11(RNAi)[c]	0	0	100 (45)	0	0	100 (20)
pgp-12(gk19)	0	0	100 (40)	0	0	100 (25)
pgp-13(ok747)	0	0	100 (50)	0	0	100 (20)
pgp-14(RNAi)[c]	0	0	100 (40)	0	0	100 (25)
pgp-15(ok987)	0	0	100 (50)	0	0	100 (20)
haf-1(ok705)	0	0	100 (50)	0	0	100 (25)
haf-2(gk13)	0	0	100 (50)	0	0	100 (20)
haf-3(ok1086)	0	0	100 (57)	0	0	100 (25)
haf-4(gk240)	53	31	16 (55)	0	0	100 (25)
haf-5/lmt-1(gk155)	0	0	100 (55)	0	0	100 (25)
haf-5/lmt-1(gk161)	5	0	95 (56)	0	0	100 (24)
haf-7(gk46)	0	0	100 (50)	0	0	100 (25)
haf-8(gk12)	0	0	100 (50)	0	0	100 (20)
haf-9(gk23)	2	0	98 (47)	0	0	100 (20)
Double mutant analysis[e]						
apt-6(ok429)	5	82	13 (98)	0	100	0 (25)
apt-6(ok429) pgp-2(kx48)	99	1	0 (86)	100	0	0 (25)
apt-7(tm920)	10	88	2 (98)	0	100	0 (25)
apt-7(tm920); pgp-2(kx48)	93	7	0 (92)	100	0	0 (25)
apt-7(tm920); pgp-2(kx55)	100	0	0 (72)	100	0	0 (28)
glo-1(zu437)	100	0	0 (84)	100	0	0 (20)
glo-1(zu437); pgp-2(kx48)	100	0	0 (65)	100	0	0 (27)
glo-4(ok623)	100	0	0 (64)	100	0	0 (25)
glo-4(ok623); pgp-2(kx48)	100	0	0 (71)	100	0	0 (27)

All strains were grown at 22°C. Two-fold and later stage embryos were analyzed using polarization microscopy and scored for the number of birefringent gut granules within the intestine. L4/young adults were analyzed using fluorescence microscopy with a standard fluorescein isothiocyanate (FITC) filter and were scored for the number of autofluorescent gut granules present within the intestine.

[a] Values in parentheses are the number of embryos scored.

[b] Values in parentheses are the number of animals scored.

[c] RNAi was carried out in an *rrf-3(pk1426)* RNAi-sensitive background (Simmer *et al.*, 2002).

[d] Embryos scored were the progeny of *pgp-7(ok528)/szT1* balanced strain, *pgp-7(ok528)* homozygous adults with protruding vulvas that produced dead embryos were scored.

[e] A *dpy-5(e61)* marker that did not alter the Glo phenotype was present in each strain.

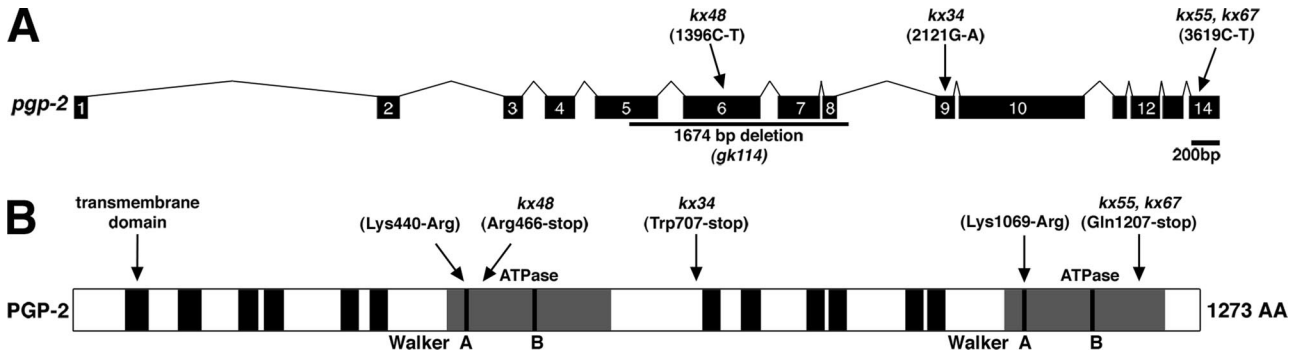

Figure 1. Structure of *pgp-2* and encoded protein. (A) The genomic structure of *pgp-2* showing the location and specific changes of *pgp-2* mutations. Exons are denoted by black boxes. (B) The predicted domain structure of PGP-2 showing the positions of transmembrane domains, ATPase domains, Walker A and B motifs, and *pgp-2* mutations.

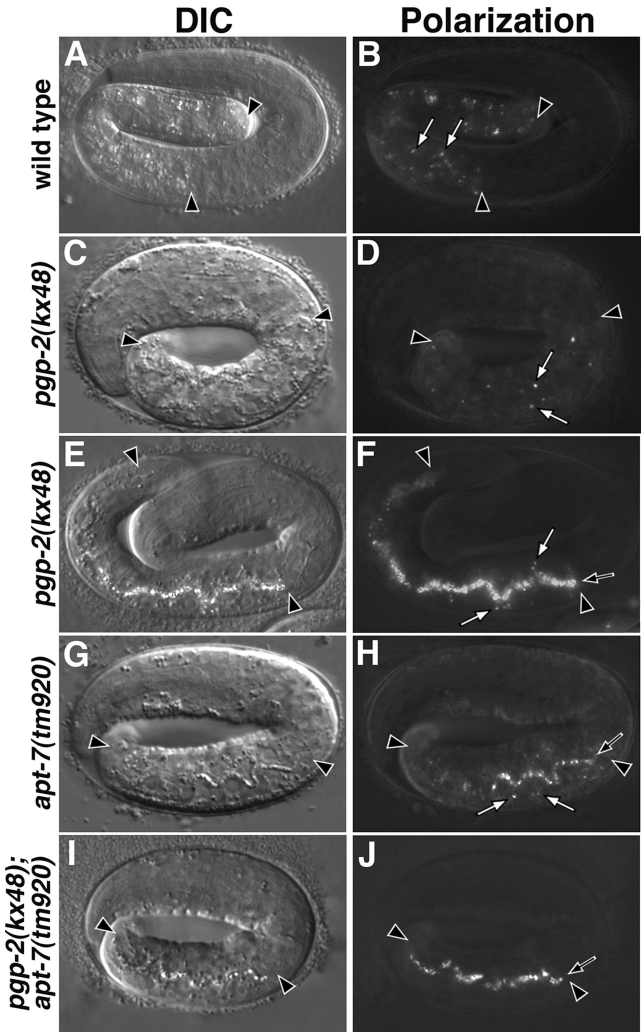

Figure 2. Analysis of birefringent granules in embryos. Birefringent granules (white arrows) are present within intestinal cells in wild-type pretzel-stage embryos (A and B). Early pretzel-stage *pgp-2(−)* embryos (C and D) contained reduced numbers of birefringent granules within intestinal cells. Late pretzel-stage *pgp-2(−)* embryos (E and F) contained reduced numbers of birefringent granules within intestinal cells and birefringent material within the intestinal lumen (black arrow). *apt-7(−)* late pretzel-stage embryos (G and H) contained birefringent granules in the intestinal lumen (black arrow) and reduced numbers of birefringent granules in intestinal cells. *pgp-2(−); apt-7(−)* late pretzel-stage embryos contained birefringent material within the intestinal lumen (black arrow) and lacked birefringent granules within intestinal cells. Intestinal cells are located between the black arrowheads in all panels. *C. elegans* embryos are ~50 μm in length.

birefringent material in *pgp-2(−)* embryonic intestinal cells. In wild-type 1.5-fold– and pretzel-stage embryos (Figure 3, U and V), 95% (n = 114) and 98% (n = 252) of birefringent puncta were stained by the lysosomal marker acridine orange, respectively. Thirty-two percent (n = 38) of birefringent puncta in *pgp-2(−)* 1.5-fold–stage embryos were stained by acridine orange, and 99% (n = 122) of birefringent puncta were stained by acridine orange in *pgp-2(−)* pretzel-stage embryos 99% (n = 122; Figure 3, W and X). However, the staining of these compartments by acridine orange was weaker than wild type (Figure 3, A, B, U, and W). We examined the endocytic membrane markers RAB-5::GFP, RAB-7::GFP, and LMP-1::GFP (Chen *et al.*, 2006) for their presence around birefringent puncta. In wild-type pretzel-stage embryos, birefringent material was rarely found within RAB-5::GFP (1%, n = 142), RAB-7::GFP (0.5%, n = 227), or LMP-1::GFP (3%, n = 245) containing organelles. In *pgp-2(−)* embryonic intestinal cells, birefringent material did not colocalize with RAB-5::GFP (not shown). However, a minor proportion of birefringent puncta in *pgp-2(−)* pretzel-stage embryos colocalized with LMP-1::GFP (20%, n = 55) and RAB-7::GFP (12%, n = 57; not shown). Although there are GLO-1::GFP puncta in *pgp-2(−)* embryos (Figure 3H), we were unable to analyze their localization relative to birefringent material because of a genetic interaction between *glo-1::gfp* and *pgp-2(kx48)* that resulted in the complete lack of birefringent material in the intestinal cells of *pgp-2(kx48); glo-1::gfp* embryos (data not shown). We have recently identified a predicted membrane associated protein encoded by *glo-3* (Hermann *et al.*, 2005) that localizes to the gut granule membrane (Rabbitts and Hermann, unpublished results). In wild-type 1.5-fold– and pretzel-stage embryos, 80% (n = 79) and 76% (n = 137) of birefringent puncta colocalized with GLO-3::GFP (not shown), respectively. In contrast, only 7% (n = 55) of birefringent puncta in *pgp-2(−)* 1.5-fold–stage embryos and 12% (n = 51) of birefringent puncta in *pgp-2(−)* pretzel-stage embryos colocalized with GLO-3::GFP (not shown).

To determine whether the formation of birefringent puncta in *pgp-2(−)* embryonic intestinal cells required the activity of genes that function in gut granule biogenesis, we generated double mutants between *pgp-2* and *glo-1* or *glo-4*. *glo-4* encodes a putative guanine nucleotide exchange factor for GLO-1, and *glo-4(−)* and *glo-1(−)* embryos lack birefringent gut granules (Hermann *et al.*, 2005). We found that *pgp-2(−); glo-1(−)* and *pgp-2(−); glo-4(−)* mutants lacked embryonic birefringent granules (Table 1), indicating that *glo-1* and *glo-4* are necessary for the formation of birefringent organelles in *pgp-2(−)*. Together these data indicate that the birefringent material in *pgp-2(−)* embryos is contained within endolysosomal compartments, possibly aberrantly formed gut granules.

We examined whether *pgp-2* was necessary for the formation of other endolysosomal organelles in *C. elegans* embryos. In wild type, the early endosome-associated proteins RME-1::GFP (Grant *et al.*, 2001), RAB-5::GFP (Chen *et al.*, 2006), and VPS-27 (Roudier *et al.*, 2005) were localized to punctate structures present throughout the cytoplasm or enriched near the apical surface of embryonic intestinal cells (Figure 3, I, K, and S); identical distributions were seen in *pgp-2(−)* embryos (Figure 3, J, L, and T). In intestinal cells, LMP-1::GFP (Hermann *et al.*, 2005; Chen *et al.*, 2006) is associated with the basolateral plasma membrane and what are likely endosomal compartments localized near the apical membrane (Figure 3M). This distribution was unchanged in *pgp-2(kx48)* embryos; however, some of the LMP-1::GFP containing compartments near the apical surface appeared slightly enlarged (Figure 3N). A similar phenotype is seen in *glo-1* (Hermann *et al.*, 2005) and *glo-3* (Kokes and Hermann, unpublished results) mutants; however, the cellular basis of this effect is currently unknown. RME-8::GFP (Zhang *et al.*, 2001) and RAB-7::GFP (Chen *et al.*, 2006) localize to what are likely late endosomes in embryonic intestinal cells (Figure 3, K and O). The distribution of these proteins was unaltered in *pgp-2(kx48)* embryos (Figure 3, L and P). These results suggest that despite defects in gut granule biogenesis, many aspects of the endosomal system are properly organized in *pgp-2(−)* embryos.

We next asked whether *pgp-2* was necessary for the formation of gut granules in L4 and adult stage animals. At these

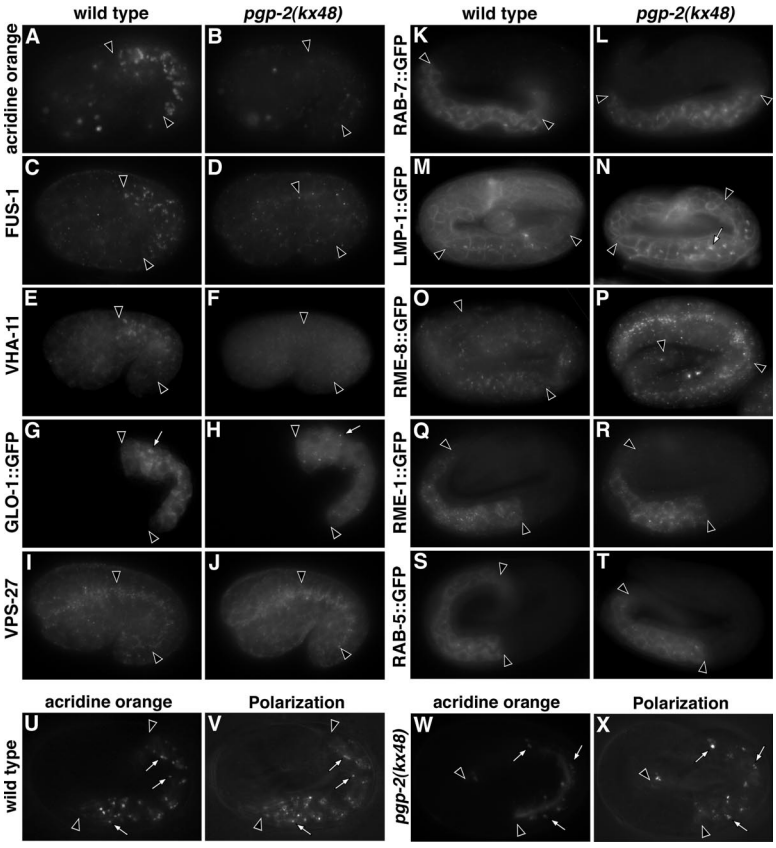

Figure 3. Analysis of endolysosomal organelles in *pgp-2(−)* embryos. Intestinal cells in wild-type 1.5-fold–stage embryos contained acridine orange–stained, acidified compartments (A) that were significantly reduced in both number and intensity in similarly staged *pgp-2(−)* embryos (B). Wild-type 1.5-fold–stage embryos contained intestinal organelles stained with anti-FUS-1 (C) and anti-VHA-11 antibodies (E) that were not present in *pgp-2(−)* embryos (D and F). Compared with wild type (G), the number and morphology of organelles marked with GLO-1::GFP (white arrows) was dramatically reduced and altered in *pgp-2(−)* embryos (H). Antibodies that recognize VPS-27 stained similar organelles in 1.5-fold–stage wild-type (I) and *pgp-2(−)* (J) embryos. Anti-GFP antibody staining was used to analyze wild-type and *pgp-2(−)* pretzel-stage embryos expressing RAB-7 (K and L), LMP-1 (M and N), RME-8 (O and P), RME-1 (Q and R), and RAB-5 (S and T) GFP fusion proteins. The appearance of organelles marked by these proteins was unaltered in *pgp-2(−)* with the exception of LMP-1::GFP, which was localized to slightly enlarged organelles in *pgp-2(−)* embryos (white arrow in N). In both wild-type (U and V) and *pgp-2(−)* (W and X) pretzel-stage embryos, birefringent material is present within acidified intestinal organelles (white arrows). Intestinal cells are located between the black arrowheads.

stages, wild-type intestinal cells contain hundreds of gut granules characterized by their autofluorescent contents, acidity, and function as terminal endocytic compartments (Clokey and Jacobson, 1986; Figure 4, B, D, and F). *pgp-2(−)* animals contained reduced numbers of organelles with diminished levels of autofluorescent material in intestinal cells, which was only faintly visible with standard FITC fluorescence filter sets (Figure 5I) and was not visible with filter sets used to visualize rhodamine fluorescence (Figures 4H and 9B). Despite containing autofluorescent organelles, L4 and adult stage *pgp-2(kx48)* animals completely lacked acidified gut granules stained by Lysotracker Red (Figure 4J) or acridine orange (Figure 9D and Table 2). TRITC-bovine serum albumen (BSA; Figure 4L) and TRITC-dextran (not shown) fed to *pgp-2(kx48)* animals was endocytosed by intestinal cells, indicating that *pgp-2* is not essential for fluid-phase endocytosis across the apical plasma membrane. However, the markers did not accumulate to the same level as in wild-type animals (Figure 4, F and L), and we therefore cannot rule out the possibility that the rate of endocytosis is reduced or the rate of endocytic recycling is increased in *pgp-2(kx48)* adults. The endocytosed TRITC-BSA signal did not localize to the autofluorescent organelles in *pgp-2(kx48)* (not shown) as they do in wild type (Clokey and Jacobson, 1986). Together, these data suggest that the autofluorescent material in *pgp-2(−)* intestinal cells is contained within aberrantly formed gut granules. Consistent with this idea, we found that *pgp-2(−); glo-1(−)* and *pgp-2(−); glo-4(−)* adults lacked autofluorescent material in their intestinal cells (Table 1). We conclude that mutations in *pgp-2* disrupt adult gut granule formation.

While this article was in preparation Nunes *et al.* (2005) similarly showed the lack of acidified compartments in *pgp-*

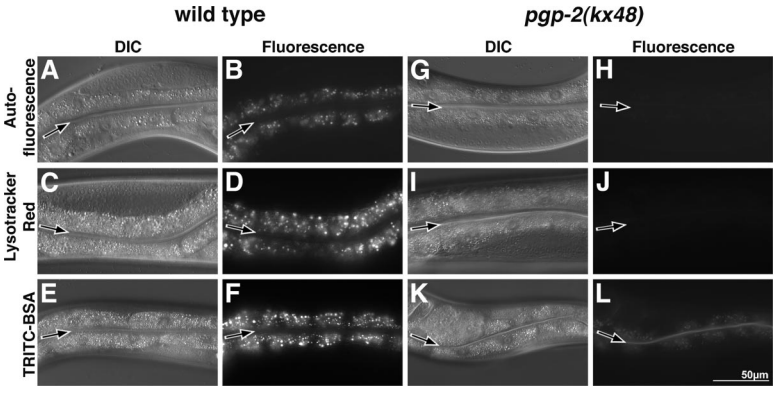

Figure 4. Analysis of autofluorescent, acidified, and terminal endocytic compartments in intestinal cells of L4/adult stage *pgp-2(−)* animals. The autofluorescent contents of wild-type gut granules are visible in the rhodamine channel (B). After staining wild type with dyes that label acidified (D) or terminal endocytic compartments (F), gut granules displayed brighter fluorescence. The intestinal cells of *pgp-2(kx48)* animals did not contain autofluorescent material visible in the rhodamine channel (H), and they did not stain with the acidic marker Lysotracker Red (J). The endocytic marker TRITC-BSA accumulated in *pgp-2(kx48)* intestinal cells at much lower levels than wild type (compare F and L). Fluorescence images of wild-type and *pgp-2(kx48)* were captured using the same exposure time. The intestinal lumen is marked with a black arrow.

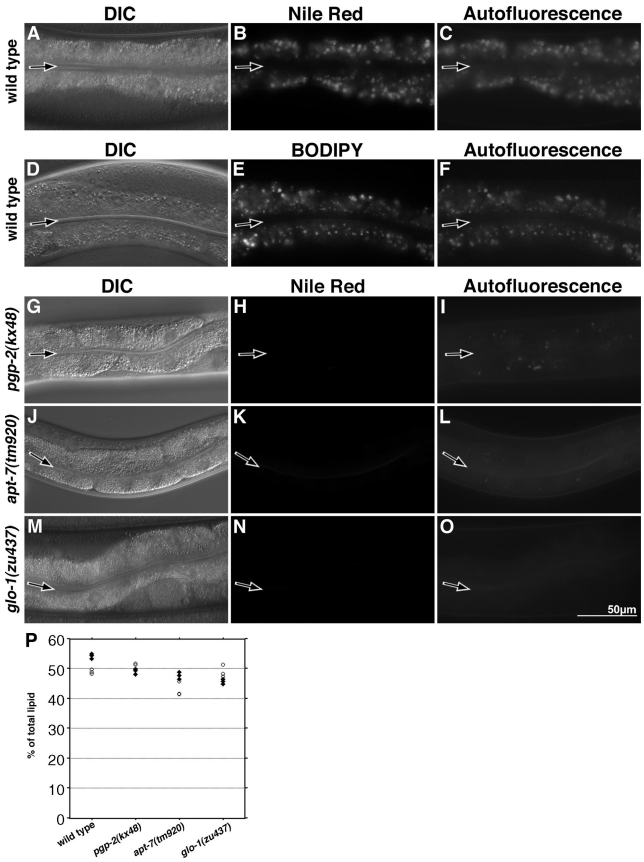

Figure 5. Gut granules are sites of fat storage in adults. The Nile Red–stained compartments of wild-type adult intestinal cells are visible in the rhodamine channel (B). These correspond to autofluorescent gut granules visible in the FITC channel (C). The BODIPY 493/503-stained compartments of wild-type adult intestinal cells are visible in the FITC channel (E). These correspond to autofluorescent gut granules visible in the rhodamine channel (F). The intestinal cells of adult *pgp-2(kx48)* animals did not contain Nile Red–stained compartments (H); however, a reduced number of weakly autofluorescent compartments were visible in the FITC channel (I). Both *apt-7(tm920)* (K) and *glo-1(zu437)* (N) adult intestinal cells lacked Nile Red–stained compartments. Fluorescence images of Nile Red staining in wild type and Glo mutants were captured using the same exposure time. The intestinal lumen is marked with a black arrow. (P) The triacylglyceride content of young adults was measured in triplicate by gas chromatography from two separate extractions. ◇ and ○, values from the first and second extractions, respectively.

2(−) adults. However, in contrast to our findings, *pgp-2(−)* animals were reported to be unable to internalize FITC-dextran. Possibly, low levels of endocytosed material were not apparent in the studies of Nunes *et al.* because of the presence of weakly autofluorescent organelles in *pgp-2(−)* that are visible with standard FITC filter sets (Figure 5I).

The Role of ABCB Transporters in Gut Granule Biogenesis

We examined whether any other transporters in the ABCB subfamily were necessary for gut granule biogenesis. The *C. elegans* genome encodes 24 members of the ABCB subfamily (Sheps *et al.*, 2004). Fifteen ABCB transporters, denoted PGP, have a domain structure similar to PGP-2 (Figure 1). The remaining nine transporters, denoted HAF, contain 4–8 transmembrane domains followed by a cytoplasmic ATPase domain. We analyzed mutations and/or RNAi of 23 ABCB subfamily transporters for alterations in the number, placement, or morphology of gut granules. Only one ABCB transporter, in addition to *pgp-2*, showed a Glo phenotype. Eighty-four percent of *haf-4(gk240)* embryos lacked or contained significantly reduced numbers of birefringent intestinal granules (Table 1). However, *haf-4(−)* embryos did not mislocalize birefringent material to the intestinal lumen and displayed FUS-1–containing and acidified organelles similar in number and distribution to gut granules in wild type (not shown). In addition, *haf-4(−)* adult autofluorescent gut granules were acidified and were indistinguishable from wild type (not shown). These data indicate that *haf-4(+)* activity controls the formation of birefringent material rather than the biogenesis of acidified gut granule per se. Intriguingly, the human gene ABCB9/TAPL, which is homologous to *haf-4*, encodes a lysosomal transporter (Zhao *et al.*, 2006), suggesting the possibility that *haf-4* mediates transport across the gut granule membrane to facilitate the formation of birefringent material. Together, our analyses indicate that the ABCB subfamily of transporters do not play a general role in *C. elegans* gut granule biogenesis and suggest that PGP-2 uniquely functions in the formation of gut granules.

pgp-2 Acts in Parallel to AP-3

The requirement of *glo-1* and *glo-4* in the generation of birefringent and autofluorescent material within *pgp-2(−)* intestinal cells (Table 1) strongly suggests that pathways for gut granule biogenesis are still functional in *pgp-2(−)* animals. To identify specific gut granule trafficking pathways that are acting in *pgp-2(−)* animals, we investigated the

Table 2. Rescue of *pgp-2(kx48)*

Genotype	Autofluorescent organelles	Acridine orange–stained organelles	Nile Red–stained organelles
Wild type	+++ (18)	+++ (20)	+++ (17)
pgp-2(kx48)	− (22)	− (19)	− (27)
pgp-2(kx48) + *vha-6::pgp-2::gfp*	+++ (23)	+++ (46)	+++ (16)
pgp-2(kx48) + *unc-119::pgp-2::gfp*	− (22)	− (30)	− (32)
pgp-2(kx48) + *vha-6::pgp-2(K440R)::gfp*	+ (37)[a]	− (19)	+ (17)[b]
pgp-2(kx48) + *vha-6::pgp-2(K1069R)::gfp*	+ (20)[a]	− (15)	+ (22)[b]
pgp-2(kx48) + *vha-6::pgp-2(K440R; K1069R)::gfp*	+ (20)[a]	− (19)	+ (19)[b]

All strains were grown at 22°C. L4/young adults were analyzed using fluorescence microscopy for autofluorescent, acridine orange, and Nile Red signals in intestinal cells using a standard rhodamine filter. Animals were scored for the number of fluorescent organelles present within the intestine. +++, ++, +, and − correspond to >500, 51–500, 1–50, and 0 organelles, respectively. Values in parentheses are the number of animals scored.

[a] *pgp-2* point mutants contained weakly autofluorescent compartments compared with wild type.

[b] *pgp-2* point mutants contained weakly stained Nile Red–stained compartments compared with wild type.

functional relationship between *pgp-2* and AP-3 in the formation of the birefringent and autofluorescent material normally localized within the gut granule (Hermann *et al.*, 2005). The *C. elegans* AP-3 adaptor complex is composed of four proteins, including the β3 and μ3 subunits encoded by *apt-6* and *apt-7* (Boehm and Bonifacino, 2001), respectively. The AP-3 complex mutants, like *pgp-2(−)*, contained reduced numbers of birefringent granules and autofluorescent organelles (Table 1 and Figures 2H and 5L) and lack acidified intestinal compartments (Hermann *et al.*, 2005). We found that *pgp-2(kx48) apt-6(ok429)*, *pgp-2(kx48); apt-7(tm920)*, and *pgp-2(kx55); apt-7(tm920)* double mutants always lacked birefringent and autofluorescent organelles (Table 1 and Figure 2J). These synthetic phenotypes indicate that AP-3 and *pgp-2(+)* have independent functions in the formation of birefringent and autofluorescent material and suggest that PGP-2 acts in parallel to the AP-3 adaptor complex in the formation of gut granules.

Gut Granules Are Sites of Fat Storage in C. elegans

pgp-2(+) activity has been implicated in regulating *C. elegans* adult fat storage. *pgp-2(RNAi)* (Ashrafi *et al.*, 2003), *pgp-2(gk114)* (Nunes *et al.*, 2005), and *pgp-2(kx48)* (Figure 5H) adults have greatly diminished staining by Nile Red, a fluorescent vital dye that marks fat storage compartments, which are mainly found in the intestinal cells of *C. elegans* (Ashrafi *et al.*, 2003; McKay *et al.*, 2003). Given the requirement of *pgp-2(+)* activity for both gut granule biogenesis and the formation of fat storage compartments in intestinal cells, we investigated whether gut granules are sites of fat storage. We examined L4/adult stage animals and found that Nile Red staining coincided with gut granule autofluorescence (Figure 5, B and C). Moreover, in 1.5-fold–stage embryos (not shown), pretzel-stage embryos (Figure 6, A–C), and newly hatched L1 stage larvae (not shown), Nile Red staining was limited to the intestine and coincided with birefringent gut granules. Identical results were seen with the neutral lipid stain BODIPY 493/503 (Gocze and Freeman, 1994; Figures 5, D–F, and 6, D–F). In 1.5-fold–stage embryos, Nile Red–stained fat was contained within gut granules marked with GLO-1::GFP (Figure 6, P–R). We conclude that fat is contained within gut granules in wild-type embryos and adults.

If gut granules are sites of fat storage, then animals defective in their formation should have reduced numbers of Nile Red–stained compartments. Mutations in *glo-1* and *apt-7* resulted in adults that lacked Nile Red–stained compartments within their intestinal cells (Figure 5, K and N). Pretzel stage *pgp-2(−)* (Figure 6H) and *apt-7(−)* (Figure 6K) embryos contained greatly reduced numbers of Nile Red–stained compartments in their intestinal cells. The intestinal cells within *glo-1(−)* pretzel-stage embryos completely lacked Nile Red staining (Figure 6N). All three Glo mutants mislocalized fat extracellularly into the embryonic intestinal lumen (Figure 6, H, K, and N).

To determine whether *glo* mutants contain reduced levels of fat, total lipids were extracted from wild-type and mutant animals, separated by TLC, and quantified by gas chromatography. Levels of triacylglycerides, which are likely the major form of stored fat in *C. elegans* (Ashrafi *et al.*, 2003), were not obviously altered in *pgp-2(−)* and *glo-1(−)* relative to wild- type (Figure 5P). *apt-7(−)* animals displayed a slight decrease in the level of triacylglycerides; triacylglycerides as a mean percentage of total lipids were as follows: wild type 52%, *pgp-2(kx48)* 50%, *apt-7(tm920)* 45%, and *glo-1(zu437)* 47%. We did not detect any alterations in the levels of specific fatty acids in the *glo* mutants (not shown). These data indicate that the loss of Nile Red staining does not necessarily correlate with a significant decrease in the level of fat at the level of the organism.

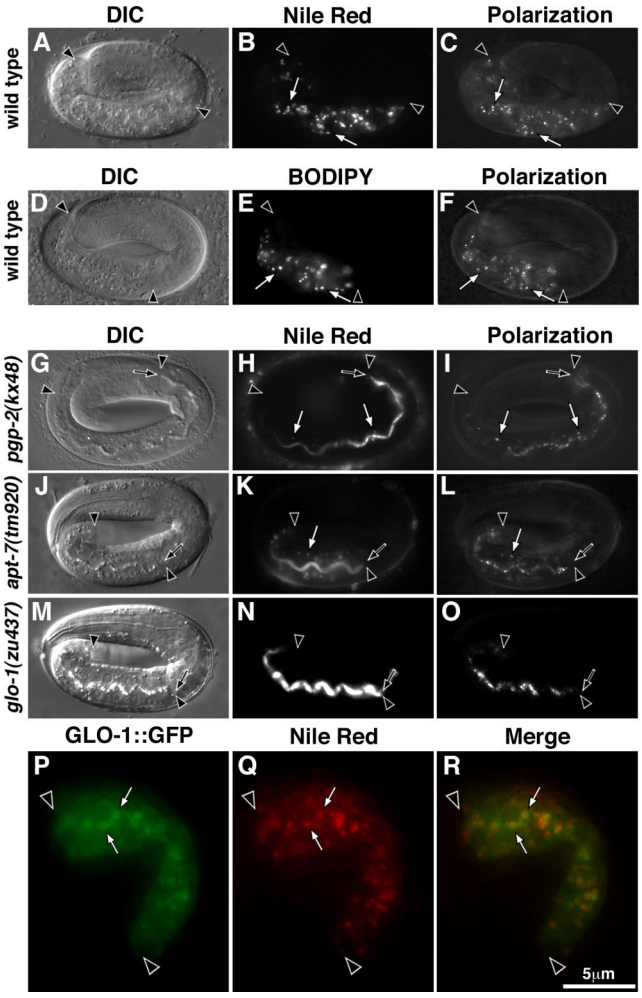

Figure 6. Gut granules are sites of fat storage in embryos. Nile Red– (B) and BODIPY493/503 (E)-stained, fat-containing compartments colocalized (white arrows) with birefringent gut granules in wild-type pretzel-stage (C and F) embryos. Pretzel stage *pgp-2(kx48)* and *apt-7(tm920)* embryos contain a significantly reduced number of Nile Red–stained compartments and mislocalize Nile Red–stained fat into the intestinal lumen (H and K). The Nile Red staining in *pgp-2(kx48)* and *apt-7(tm920)* intestinal cells colocalized with birefringent material (white arrows in H–I and K–L). The intestinal cells of *glo-1(zu437)* pretzel-stage embryos lack Nile Red–stained compartments and mislocalize Nile Red–stained fat into the intestinal lumen (N and O). In a 1.5-fold–stage embryo expressing the gut granule–associated protein GLO-1::GFP, Nile Red staining is contained within GLO-1::GFP marked organelles (P–R). Intestinal cells are located between black arrowheads and the intestinal lumen is marked with a black arrow.

PGP-2 Is Expressed in the Intestine and Localized to the Gut Granule Membrane

We investigated *pgp-2* expression by using a *gfp* reporter expressed under the control of the *pgp-2* promoter (*pgp-2::gfp*). Prior analysis has reported *pgp-2::gfp* expression in pharngeal and AWA neuronal cells; however, the design of *pgp-2* reporter constructs used in prior studies was based on an incorrectly predicted first exon (Zhao *et al.*, 2004; Nunes *et al.*, 2005). Our cDNA analysis showed that exon 1

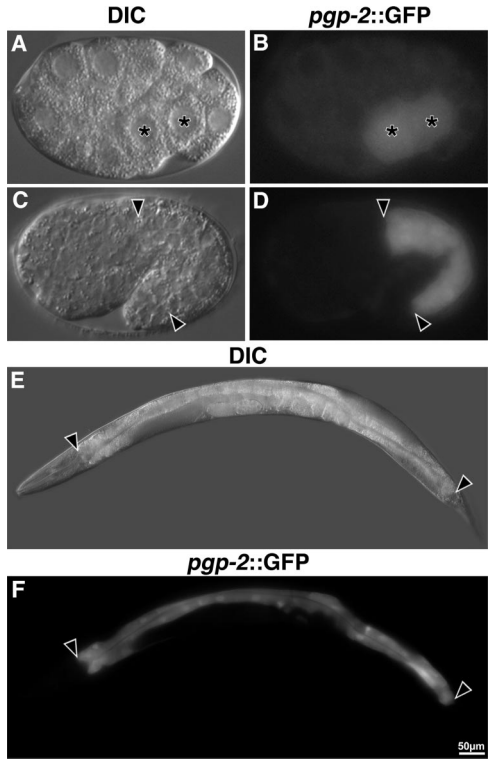

Figure 7. *pgp-2* is expressed in embryonic and adult intestinal cells. Shown are strains containing the *pgp-2* promoter driving the expression of *gfp* (*pgp-2::gfp*) from an extrachromosomal transgene. Expression of *gfp* in E2 (A and B) and 1.5-fold–stage (C and D) embryos are shown. In A and B, asterisks mark the nuclei of the intestinal precursors. *gfp* was expressed within the adult intestine (E and F). In C–F, intestinal cells are located between the black arrowheads.

of *pgp-2* is encoded 2.2 kb upstream of the predicted exon 1 (Wormbase WS160). We placed *gfp* under the control of a 7.6-kb sequence that extends from the predicted upstream gene C34G6.6 to the new predicted start codon of *pgp-2*. Embryonic expression of *pgp-2::gfp* was first seen in the daughters of the E blastomere (E^2 stage), which generate the intestine (Figure 7B). Intestinal expression persisted through embryogenesis (Figure 7D) and into adulthood (Figure 7F). Rarely, weak expression of *pgp-2::gfp* was detected in embryonic and adult hypodermal cells (not shown). We never detected pharyngeal or AWA expression of the *pgp-2::gfp* reporter.

We analyzed the localization of PGP-2 with anti-PGP-2 antibodies and an amino terminally tagged PGP-2::GFP fusion expressed under the control of the intestinal specific *vha-6* promoter (Oka *et al.*, 2001; Pujol *et al.*, 2001). The PGP-2::GFP fusion rescued the loss of autofluorescence, Nile Red–stained fat, and acridine orange–stained acidified compartments in *pgp-2(kx48)* (Figure 9, G–L, and Table 2). This rescuing activity indicates that expression of *pgp-2(+)* in the intestine is sufficient for its function in gut granule biogenesis and fat storage. Expression of PGP-2::GFP under the control of the pan-neuronally expressed *unc-119* promoter (Maduro and Pilgrim, 1995) did not result in rescue of *pgp-2(−)* (Table 2). Intestinally expressed PGP-2::GFP was localized to prominent vesicular structures and the plasma membrane in embryos and adults (Figure 8, J, N, and Q). Similar organelles were stained by anti-PGP-2 antibodies (Figure 8, A and B). These structures were not present in *pgp-2(kx48)* embryos (Figure 8, C and D). Anti-PGP-2 antibodies only stained intracellular compartments in embryos and adults (not shown), suggesting that the PGP-2::GFP might be partially mislocalized to the plasma membrane. PGP-2::GFP colocalized with birefringent material (Figure 8, M–P) and the V-ATPase subunit FUS-1 in embryos (Figure 8, I–L), and in adults PGP-2::GFP colocalized with autofluorescent compartments (Figure 8, Q–S). PGP-2 antibodies stained compartments containing GLO-1::GFP (Figure 8, E–H). These results indicate that PGP-2 and PGP-2::GFP are associated with the gut granule membrane.

Mutations in PGP-2 Predicted To Block ATPase Activity Disrupt Gut Granule Biogenesis

We determined whether the hydrolytic activity of the two ATPase domains of *pgp-2* is functionally important for gut granule formation. Structural studies suggest that the Walker A motif $GX_4GKS(S/T)$ interacts with the β and γ phosphates of ATP (Schneider and Hunke, 1998). Changing the lysine to arginine in the Walker A motif of ABC transporters disrupts ATP hydrolysis (Schneider and Hunke, 1998), and mutating the conserved lysine to arginine in one or both ATPase domains has been shown to disrupt the transport activity of P-glycoprotein (Azzaria *et al.*, 1989), MDR3 (Urbatsch *et al.*, 1998), and STE-6 (Berkower and Michaelis, 1991). The lysine residue in the Walker A motif of each or both ATPase domain of PGP-2 was changed to arginine by site directed mutagenesis (Figure 1B). When introduced into wild type, the PGP-2(K440R)::GFP, PGP-2(K1069R)::GFP, and PGP-2(K440R; K1069R)::GFP proteins localized to the gut granule and plasma membranes (not shown). These mutant proteins failed to restore gut granules in *pgp-2(kx48)* adults (Figure 9, M–R), indicating that ATP hydrolysis and likely transport activity is important for PGP-2 function in gut granule biogenesis. Their expression did not rescue the loss of acidified compartments in *pgp-2(−)* animals (Figures 9, M–R; Table 2, not shown). However, each mutant promoted the formation a few weakly autofluorescent and weakly Nile Red–stained compartments (Figures 9, M–R; Table 2, not shown), indicating that they contain some residual activity.

DISCUSSION

ABC Transporters in Lysosome Biogenesis

We have shown that the ABC transporter PGP-2 plays an important role in lysosome-related organelle biogenesis in *C. elegans*. Gut granules are acidified, terminal endocytic, fat containing, lysosome-related organelles with birefringent and autofluorescent contents (Clokey and Jacobson, 1986; Hermann *et al.*, 2005, this work). Disrupting *pgp-2(+)* activity results in the partial mislocalization of birefringent material into the embryonic intestinal lumen (Figure 2). This phenotype resembles the secretion of lysosomal contents that results from defects in trafficking to yeast or mammalian lysosomes (Kornfeld and Mellman, 1989; Mullins and Bonifacino, 2001). Indeed, the activity of three *C. elegans* genes encoding proteins implicated in vesicle trafficking (a Rab GTPase and two subunits of the AP-3 complex) result in the similar extracellular mislocalization of birefringent material (Hermann *et al.*, 2005). Mutations in *pgp-2* also lead to defects in the formation of acidified gut granules. In intestinal cells at the 1.5-fold stage, subunits of the V-ATPase are enriched on gut granule membranes (Oka and Futai, 2000; Hermann *et al.*, 2005). Similarly staged *pgp-2(−)* embryos lacked detectable expression of two V-ATPase subunits and had greatly reduced numbers of acidified compartments in

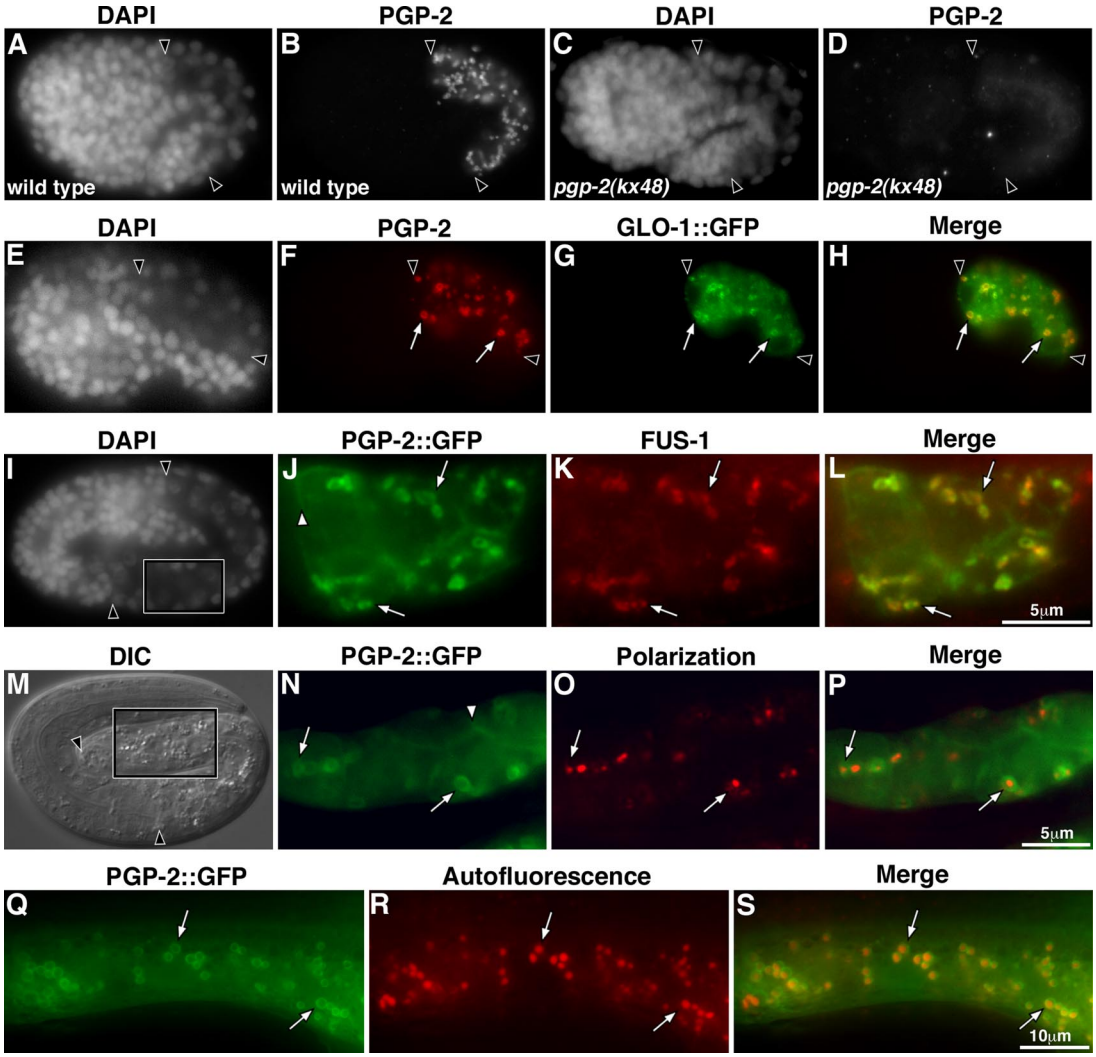

Figure 8. PGP-2 is localized to the gut granule membrane. Anti-PGP-2 antibody staining of wild type (A and B) and *pgp-2(kx48)* (C and D) 1.5-fold–stage embryos. (E and H) Anti-PGP-2 and anti-GFP antibody staining of a GLO-1::GFP-expressing bean stage embryo. PGP-2 and GLO-1::GFP colocalized to the same intestinal organelles (white arrows). (I–P) Pretzel stage embryos carrying an extrachromosomal transgene containing the *vha-6* promoter driving the expression of PGP-2::GFP in intestinal cells. (I–L) A PGP-2::GFP-expressing embryo showing colocalization (white arrows) of staining by anti-GFP and anti-FUS-1 antibodies at high magnification (boxed region of intestine marked in I). (M–P) High magnification of the intestine of a PGP-2::GFP-expressing embryo (boxed region in M). PGP-2::GFP marked vesicles (white arrows) contain birefringent material (pseudocolored red in O and P). A minor proportion of PGP-2::GFP is localized to the plasma membrane (white arrowhead in J and N). In A–H, I, and M intestinal cells are located between the black arrowheads. (Q–S) An intestinal cell in a *pgp-2(kx48)* adult expressing PGP-2::GFP under control of the *vha-6* promoter. PGP-2::GFP is localized to membranes surrounding autofluorescent material visible in the rhodamine channel (white arrows).

embryonic intestinal cells (Figure 3). As reported previously by Nunes *et al.* (2005), we found that *pgp-2(−)* adults lacked acidified intestinal organelles (Figure 4).

The gut granule biogenesis pathways involving the GLO-1 Rab GTPase and the AP-3 complex appear to be active in *pgp-2(−)* animals. Late-stage *pgp-2(−)* embryos still are able to generate a limited number of birefringent compartments that are acidified (Figure 3), fat containing (Figure 6), and not marked with the gut granule protein GLO-3::GFP (data not shown). *pgp-2(−)* adults contain a limited number of organelles with weakly autofluorescent material; however, they are not acidified and do not act as terminal endocytic compartments (Figure 4). Currently, the identity of most of the compartments containing birefringent and autofluorescent material in *pgp-2(−)* is unclear. However, their formation depends upon GLO-1, GLO-4, and subunits of the AP-3 complex (Table 1), raising the possibility that they might represent aberrantly formed gut granules. Interestingly, the AP-3 complex mutants, like *pgp-2(−)* contain, reduced numbers of compartments containing birefringent material, autofluorescent material, and fat (Figures 3 and 6 and Table 1). The formation of these organelles in AP-3 complex mutants requires *pgp-2(+)* activity (Figure 3 and Table 1), suggesting that PGP-2 functions independently of, and possibly in parallel to, the AP-3 adaptor complex to facilitate gut granule biogenesis.

Prior studies led to the proposal that *pgp-2* functions in a subset of neuronal cells to specifically control acidification of intestinal organelles and that *pgp-2(+)* activity is not necessary for lysosomal biogenesis (Nunes *et al.*, 2005). The conclusion that *pgp-2* is expressed in a few chemosensory neurons and not in the intestine is based upon a reporter lacking

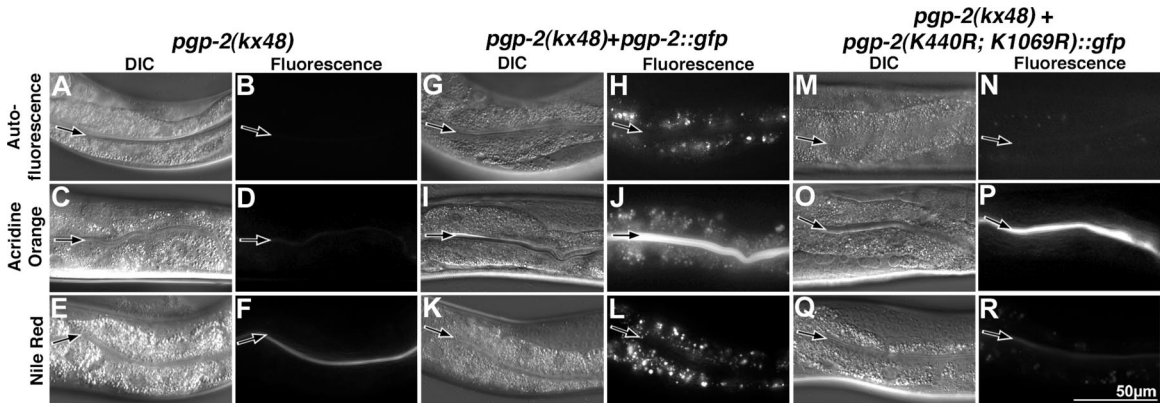

Figure 9. Rescue of autofluorescent, acidified, and fat-containing compartments in *pgp-2(−)* adults. *pgp-2(kx48)* lacked autofluorescent material visible in the rhodamine channel (B) and did not stain with the dyes that label acidified (D) or fat-containing compartments (F). *pgp-2(kx48)* animals expressing PGP-2::GFP under the control of the intestinal specific *vha-6* promoter contained autofluorescent (H), acidified (J), and fat-containing (L) compartments. *pgp-2(kx48)* animals expressing PGP-2(K440R; K1069R)::GFP lacked acidified compartments (P) and contained a few weakly autofluorescent (N) and weakly Nile Red–stained organelles (R). Images of each type of fluorescent dye were captured using the same exposure time. The intestinal lumen is marked with a black arrow.

the entire *pgp-2* promoter. Our transcriptional reporter, which was designed based on experimental determination of the start of the *pgp-2* coding sequence, indicates that *pgp-2* is expressed in the intestine and not in chemosensory neurons (Figure 7). Furthermore, using tissue specific promoters we show that *pgp-2* expression in the intestine, and not the nervous system, is sufficient for its function in gut granule biogenesis (Table 2 and Figure 9). The conclusion that PGP-2 is not required for lysosome biogenesis is based on the unaltered localization and morphology of the presumed lysosomal associated membrane protein LMP-1::GFP (Kostich *et al.,* 2000) in *pgp-2(−)* animals (Nunes *et al.,* 2005). However, current data indicate that LMP-1::GFP is not associated with embryonic or adult gut granules (Chen *et al.,* 2006 and our unpublished observations); instead LMP-1::GFP may be present on other endosomal compartments such as conventional lysosomes that coexist with gut granules in intestinal cells. On the basis of our results we conclude that *pgp-2* functions in intestinal cells to directly regulate the formation of gut granules.

ATP hydrolysis by ABC transporters fuels the transport of substrates across a membrane (Higgins, 1992). The *pgp-2(K440R)*, *pgp-2(K1069R)*, and *pgp-2(K440R; K1069R)* mutations in the Walker A motifs of ATPase domain similarly disrupt the function of PGP-2 in gut granule formation (Figure 9 and Table 2); however, they do not alter the localization of PGP-2::GFP to gut granules (not shown). The mutations we generated in PGP-2 are equivalent to mutations in three other ABCB proteins: P-glycoprotein (Azzaria *et al.,* 1989), MDR3 (Urbatsch *et al.,* 1998), and STE-6 (Berkower and Michaelis, 1991), that disrupt transport activity. These results strongly suggest that the role of PGP-2 in gut granule biogenesis actively involves its transporter activity.

We propose that PGP-2 regulates membrane traffic involved in gut granule biogenesis by controlling the membrane composition of the gut granule where PGP-2 is localized (Figure 8). Most eukaryotic ABC proteins act to export substrates unidirectionally across a cellular membrane (Borst and Elferink, 2002). Presently, what PGP-2 could be transporting is a matter of speculation. However, proteins within an ABC subfamily have an evolutionarily conserved propensity to transport similar substrates (Holland *et al.,* 2003). A number of ABCB subfamily proteins, of which PGP-2 is a member, transport lipids and sterols from the cytosolic to the lumenal or exoplasmic leaflet of cellular membranes (Pohl *et al.,* 2005; van Meer *et al.,* 2006). PGP-2 might therefore function to control lipid or sterol-based signals that regulate membrane trafficking by promoting their removal from the cytosolic leaflet of a cellular membrane (Downes *et al.,* 2005; Maxfield and Tabas, 2005). Alternatively, PGP-2 mediated movement of lipids or sterols from the cytosolic to luminal leaflet of a membrane could modify its physical properties to mechanically regulate membrane trafficking (Graham, 2004; McMahon and Gallop, 2005). Intriguingly, members of the Drs2 family of P-type ATPases mediate the movement of lipids from the lumenal to the cytosolic leaflet of membranes and function in vesicle transport to lysosomes in yeast (Gall *et al.,* 2002; Hua *et al.,* 2002; Wicky *et al.,* 2004). The identification and characterization of extragenic suppressors of *pgp-2(−)*, which could identify genes whose activity counteracts *pgp-2(+)*, would be a first step in discerning the molecular activity of PGP-2 in organelle biogenesis.

Recently another ABC transporter has been directly implicated in endolysosomal organelle biogenesis. ABCA3 is a lamellar body–associated lipid transporter whose inactivation results in respiratory distress syndrome (Shulenin *et al.,* 2004). RNAi-mediated knockdown of ABCA3 expression results in the loss of lamellar body–associated proteins from cells, suggestive of a defect in the biogenesis (Cheong *et al.,* 2006) of this lysosome-related organelle (Weaver *et al.,* 2002). Two other ABC transporters are implicated in trafficking through the endolysosomal pathway: MdrA1 in *Dictyostelium* localizes to endolysosomal membranes and *mdrA1(−)* cells show decreased rates of endocytosis (Brazill *et al.,* 2001); and mutations in ABCA1 cause Tangier disease and result in increased rates of endocytosis (Zha *et al.,* 2001). Presently at least nine mammalian ABC transporters, ABCA1 (Neufeld *et al.,* 2004), ABCA2 (Zhou *et al.,* 2001), ABCA3 (Yamano *et al.,* 2001), ABCA5 (Kubo *et al.,* 2005), ABCB1 (Rajagopal and Simon, 2003), ABCB9 (Zhang *et al.,* 2000), ABCC1 (Rajagopal and Simon, 2003), ABCC4 (Jedlitschky *et al.,* 2004), and ABCG2 (Rajagopal and Simon, 2003), are associated with late endosomes, lysosomes, or lysosome-related organelles. For most of these proteins it remains an open question whether they function in membrane trafficking and/or organelle biogenesis.

Gut Granules as Sites of Fat Storage

The studies presented here provide evidence that gut granules function as fat storage organelles in *C. elegans* adults and embryos. We found that two different lipid selective probes, Nile Red (Greenspan and Fowler, 1985; Greenspan *et al.*, 1985) and BODIPY 493/503 (Gocze and Freeman, 1994), stained autofluorescent gut granules of adults (Figure 5) and embryonic gut granules marked by birefringent material and GLO-1::GFP (Figure 6). Disrupting the activity of PGP-2, GLO-1, or the AP-3 adaptor complex subunit APT-7, three proteins that function in the biogenesis of acidified gut granules (this work and Hermann *et al.*, 2005) resulted in the loss or reduction of Nile Red staining in adult and embryonic intestinal cells and the mislocalization of Nile Red–stained fat into the embryonic intestinal lumen (Figures 5 and 6). Furthermore, the genomic RNAi screen performed by Ashrafi *et al.* (2003) identify four additional Glo genes, *apt-6*, *glo-3*, *glo-4*, and *vps-16* (Hermann *et al.*, 2005), as having loss of Nile Red–stained intestinal compartments. Notably, the vast majority of RNAi clones identified by Ashrafi *et al.* (2003) that cause reduced Nile Red staining in the intestine do not cause obvious defects in the formation of autofluorescent gut granules (our unpublished observations), suggesting that gut granules do not nonspecifically accumulate the Nile Red dye. We therefore conclude that fat storage in *C. elegans* is a specialized function of the gut granule and think it likely that the loss of Nile Red–stained fat exhibited by Glo mutants is a consequence of defects in properly forming gut granules.

Despite lacking Nile Red staining in intestinal cells, *glo* mutations do not or only slightly alter the overall level of fat/triacylglycerides in the animal. *pgp-2(−)*, and *glo-1(−)* contained wild-type amounts of fat, whereas *apt-7(−)* showed a slight decrease (Figure 5P). Studies to date have shown that animals with significantly decreased levels of fat are severely delayed in their development (Yang *et al.*, 2006). Consistent with our findings, the *glo* mutants we analyzed develop similarly to wild type (Hermann *et al.*, 2005 and data not shown). The lack of a pronounced decrease in fat levels when the activity of the *glo* genes is disrupted would result if the amount of fat stored in gut granules was minor relative to the overall level of fat in the animal. Alternatively, the loss of gut granules might result in the redistribution of fat to other cells types. In both cases, fat outside the gut granule would not be visible by Nile Red staining, as the *glo* mutants do not contain obvious staining with this dye elsewhere in the animal.

Plant and animals cells store fat in lipid droplets (Murphy, 2001), organelles that are structurally and functionally distinct from gut granules. Gut granules are lysosome-related organelles that are surrounded by a lipid bilayer (Leung *et al.*, 1999), act as terminal endocytic compartments (Clokey and Jacobson, 1986), and have an acidic lumen due to the activity of the V-ATPase (Oka and Futai, 2000). In contrast, lipid droplets do not have a vesicular structure and instead are composed of fatty acids, sterols, and embedded proteins surrounded by a phospholipid monolayer (Murphy, 2001). PAT family proteins specifically associate with lipid droplets in mammalian and *Drosophila* cells and are essential regulators of lipid droplet biogenesis, homeostasis, and movement (Murphy, 2001; Martin and Parton, 2005; Welte *et al.*, 2005). Genes encoding members of the PAT family are broadly conserved, being found in *Dictyostelium*, *Drosophila*, and vertebrates; however, they appear to be lacking from the *C. elegans* genome (Lu *et al.*, 2001). This raises the possibility that lipid droplets are not generated in *C. elegans*, which would represent a significant mechanistic variation in fat metabolism between *C. elegans* and other systems.

Although lysosomes are major sites of lipid degradation in eukaryotic cells, fat is typically not found in significant quantities in lysosomes because of the rapid export of the products generated during lipid catabolism (Kolter and Sandhoff, 2005). However, there are a few exceptional cases where lysosomes contain a greatly increased amount of fat. Human genetic diseases including Tay-Sachs and Niemann-Pick result from defective lipid degradation in/or lipid trafficking from lysosomes (Maxfield and Tabas, 2005). Lamellar bodies are fat containing lysosome-related organelles that function in the synthesis and secretion of lung surfactant (Weaver *et al.*, 2002). It remains to be seen whether the pathways leading to lysosomal fat accumulation in these cases resemble the pathways by which fat accumulates in *C. elegans* gut granules. Further studies of gut granules formation and function should enhance our understanding of the lysosomal processes involved in regulating fat transport and metabolism.

ACKNOWLEDGMENTS

We thank members of the Hermann, Binford, Lycan, and Reiness labs for advice and helpful discussions. We thank Marc Hammarlund for SNP mapping discussions, methods, and primer sequences. We gratefully acknowledge Masamitsu Futai, Kenji Kontani, Renaud Legouis, and Joel Rothman for gifts of antisera and Barth Grant for *C. elegans* vectors and strains. Some nematode strains were provided by the *Caenorhabditis* Genetics Center, the *C. elegans* Knockout Consortium, and the National Bioresource Project for *C. elegans*. This work was supported by grants from the National Science Foundation (MCB-0314332) to G.J.H. and the National Institutes of Health (R01-DK074114) to J.L.W.

REFERENCES

Ashrafi, K., Chang, F. Y., Watts, J. L., Fraser, A. G., Kamath, R. S., Ahringer, J., and Ruvkun, G. (2003). Genome-wide RNAi analysis of *Caenorhabditis elegans* fat regulatory genes. Nature *421*, 268–272.

Azzaria, M., Schurr, E., and Gros, P. (1989). Discrete mutations introduced in the predicted nucleotide-binding sites of the mdr1 gene abolish its ability to confer multidrug resistance. Mol. Cell. Biol. *9*, 5289–5297.

Babu, P. (1974). Biochemical genetics of *Caenorhabditis elegans*. Mol. Gen. Genet. *135*, 39–44.

Berkower, C., and Michaelis, S. (1991). Mutational analysis of the yeast a-factor transporter STE6, a member of the ATP binding cassette (ABC) protein superfamily. EMBO J. *10*, 3777–3785.

Boehm, M., and Bonifacino, J. S. (2001). Adaptins: the final recount. Mol. Biol. Cell *12*, 2907–2920.

Borst, P., and Elferink, R. O. (2002). Mammalian ABC transporters in health and disease. Annu. Rev. Biochem. *71*, 537–592.

Bossinger, O., and Schierenberg, E. (1996). The use of fluorescent marker dyes for studying intercellular communication in nematode embryos. Int. J. Dev. Biol. *40*, 431–439.

Brazill, D. T., Meyer, L. R., Hatton, R. D., Brock, D. A., and Gomer, R. H. (2001). ABC transporters required for endocytosis and endosomal pH regulation in *Dictyostelium*. J. Cell Sci. *114*, 3923–3932.

Brenner, S. (1974). The genetics of *Caenorhabditis elegans*. Genetics *77*, 71–94.

Brock, T. J., Browse, J., and Watts, J. L. (2006). Genetic regulation of unsaturated fatty acid composition in *C. elegans*. PLoS Genet *2*, e108.

Chen, C. C., Schweinsberg, P. J., Vashist, S., Mareiniss, D. P., Lambie, E. J., and Grant, B. D. (2006). RAB-10 is required for endocytic recycling in the *Caenorhabditis elegans* intestine. Mol. Biol. Cell *17*, 1286–1297.

Cheong, N., Madesh, M., Gonzales, L. W., Zhao, M., Yu, K., Ballard, P. L., and Shuman, H. (2006). Functional and trafficking defects in ATP binding cassette A3 mutants associated with respiratory distress syndrome. J. Biol. Chem. *281*, 9791–9800.

Clokey, G. V., and Jacobson, L. A. (1986). The autofluorescent "lipofuscin granules" in the intestinal cells of *Caenorhabditis elegans* are secondary lysosomes. Mech. Ageing Dev. *35*, 79–94.

Davis, M. W., Hammarlund, M., Harrach, T., Hullett, P., Olsen, S., and Jorgensen, E. M. (2005). Rapid single nucleotide polymorphism mapping in *C. elegans*. BMC Genomics *6*, 118.

Dell'Angelica, E. C. (2004). The building BLOC(k)s of lysosomes and related organelles. Curr. Opin. Cell Biol. *16*, 458–464.

Dell'Angelica, E. C., Mullins, C., Caplan, S., and Bonifacino, J. S. (2000). Lysosome-related organelles. FASEB J. *14*, 1265–1278.

Di Pietro, S. M., and Dell'Angelica, E. C. (2005). The cell biology of Hermansky-Pudlak syndrome: recent advances. Traffic *6*, 525–533.

Downes, C. P., Gray, A., and Lucocq, J. M. (2005). Probing phosphoinositide functions in signaling and membrane trafficking. Trends Cell Biol. *15*, 259–268.

Gall, W. E., Geething, N. C., Hua, Z., Ingram, M. F., Liu, K., Chen, S. I., and Graham, T. R. (2002). Drs2p-dependent formation of exocytic clathrin-coated vesicles in vivo. Curr. Biol. *12*, 1623–1627.

Gocze, P. M., and Freeman, D. A. (1994). Factors underlying the variability of lipid droplet fluorescence in MA-10 Leydig tumor cells. Cytometry *17*, 151–158.

Graham, T. R. (2004). Flippases and vesicle-mediated protein transport. Trends Cell Biol. *14*, 670–677.

Grant, B., Zhang, Y., Paupard, M.-C., Lin, S. X., Hall, D., and Hirsh, D. (2001). Evidence that RME-1, a conserved *C. elegans* EH domain protein, functions in endocytic recycling. Nat. Cell Biol. *3*, 573–579.

Greenspan, P., and Fowler, S. D. (1985). Spectrofluorometric studies of the lipid probe, nile red. J. Lipid Res. *26*, 781–789.

Greenspan, P., Mayer, E. P., and Fowler, S. D. (1985). Nile red: a selective fluorescent stain for intracellular lipid droplets. J. Cell Biol. *100*, 965–973.

Hermann, G. J., Schroeder, L. K., Hieb, C. A., Kershner, A. M., Rabbitts, B. M., Fonarev, P., Grant, B. D., and Priess, J. R. (2005). Genetic analysis of lysosomal trafficking in *Caenorhabditis elegans*. Mol. Biol. Cell *16*, 3273–3288.

Higgins, C. F. (1992). ABC transporters: from microorganisms to man. Annu. Rev. Cell Biol. *8*, 67–113.

Hobert, O. (2002). PCR fusion-based approach to create reporter gene constructs for expression analysis in transgenic *C. elegans*. BioTechniques *32*, 728–730.

Holland, I., Cole, S., Kuchler, K., and Higgins, C. (eds.) (2003). ABC Proteins: From Bacteria to Man, San Diego, CA: Elsevier Science.

Hua, Z., Fatheddin, P., and Graham, T. R. (2002). An essential subfamily of Drs2p-related P-type ATPases is required for protein trafficking between Golgi complex and endosomal/vacuolar system. Mol. Biol. Cell *13*, 3162–3177.

Huizing, M., Boissy, R. E., and Gahl, W. A. (2002). Hermansky-Pudlak syndrome: vesicle formation from yeast to man. Pigment Cell Res. *15*, 405–419.

Jedlitschky, G., Tirschmann, K., Lubenow, L. E., Nieuwenhuis, H. K., Akkerman, J. W., Greinacher, A., and Kroemer, H. K. (2004). The nucleotide transporter MRP4 (ABCC4) is highly expressed in human platelets and present in dense granules, indicating a role in mediator storage. Blood *104*, 3603–3610.

Jones, P. M., and George, A. M. (2004). The ABC transporter structure and mechanism: perspectives on recent research. Cell Mol. Life Sci. *61*, 682–699.

Kamath, R. S. *et al.* (2003). Systematic functional analysis of the *Caenorhabditis elegans* genome using RNAi. Nature *421*, 231–237.

King, S. M., and Reed, G. L. (2002). Development of platelet secretory granules. Semin. Cell Dev. Biol. *13*, 293–302.

Kolter, T., and Sandhoff, K. (2005). Principles of lysosomal membrane digestion: stimulation of sphingolipid degradation by sphingolipid activator proteins and anionic lysosomal lipids. Annu. Rev. Cell Dev. Biol. *21*, 81–103.

Kontani, K., Moskowitz, I.P.G., and Rothman, J. H. (2005). Repression of cell-cell fusion by components of the *C. elegans* vacuolar ATPase complex. Dev. Cell *8*, 787–794.

Kornfeld, S., and Mellman, I. (1989). The biogenesis of lysosomes. Annu. Rev. Cell Biol. *5*, 483–525.

Kostich, M., Fire, A., and Fambrough, D. M. (2000). Identification and molecular-genetic characterization of a LAMP/CD68-like protein from *Caenorhabditis elegans*. J. Cell Sci. *113*, 2595–2606.

Kubo, Y., Sekiya, S., Ohigashi, M., Takenaka, C., Tamura, K., Nada, S., Nishi, T., Yamamoto, A., and Yamaguchi, A. (2005). ABCA5 resides in lysosomes, and ABCA5 knockout mice develop lysosomal disease-like symptoms. Mol. Cell. Biol. *25*, 4138–4149.

Laufer, J. S., Bazzicalupo, P., and Wood, W. B. (1980). Segregation of developmental potential in early embryos of *Caenorhabditis elegans*. Cell *19*, 569–577.

Leung, B., Hermann, G. J., and Priess, J. R. (1999). Organogenesis of the *Caenorhabditis elegans* intestine. Dev. Biol. *216*, 114–134.

Li, W., Rusiniak, M. E., Chintala, S., Gautam, R., Novak, E. K., and Swank, R. T. (2004). Murine Hermansky-Pudlak syndrome genes: regulators of lysosome-related organelles. BioEssays *26*, 616–628.

Lu, X., Gruia-Gray, J., Copeland, N. G., Gilbert, D. J., Jenkins, N. A., Londos, C., and Kimmel, A. R. (2001). The murine perilipin gene: the lipid droplet-associated perilipins derive from tissue-specific, mRNA splice variants and define a gene family of ancient origin. Mamm. Genome *12*, 741–749.

Maduro, M., and Pilgrim, D. (1995). Identification and cloning of *unc-119*, a gene expressed in the *Caenorhabditis elegans* nervous system. Genetics *141*, 977–988.

Martin, S., and Parton, R. G. (2005). Caveolin, cholesterol, and lipid bodies. Semin. Cell Dev. Biol. *16*, 163–174.

Maxfield, F. R., and Tabas, I. (2005). Role of cholesterol and lipid organization in disease. Nature *438*, 612–621.

McKay, R. M., McKay, J. P., Avery, L., and Graff, J. M. (2003). *C. elegans*: a model for exploring the genetics of fat storage. Dev. Cell *4*, 131–142.

McMahon, H. T., and Gallop, J. L. (2005). Membrane curvature and mechanisms of dynamic cell membrane remodelling. Nature *438*, 590–596.

Mullins, C., and Bonifacino, J. S. (2001). The molecular machinery for lysosome biogenesis. BioEssays *23*, 333–343.

Murphy, D. J. (2001). The biogenesis and function of lipid bodies in animals, plants and microorganisms. Prog. Lipid Res. *40*, 325–438.

Neufeld, E. B. *et al.* (2004). The ABCA1 transporter modulates late endocytic trafficking: insights from the correction of the genetic defect in Tangier disease. J. Biol. Chem. *279*, 15571–15578.

Nunes, F., Wolf, M., Hartmann, J., and Paul, R. J. (2005). The ABC transporter PGP-2 from *Caenorhabditis elegans* is expressed in the sensory neuron pair AWA and contributes to lysosome formation and lipid storage within the intestine. Biochem. Biophys. Res. Commun. *338*, 862–871.

Oka, T., and Futai, M. (2000). Requirement of V-ATPase for ovulation and embryogenesis in *Caenorhabditis elegans*. J. Biol. Chem. *275*, 29556–29561.

Oka, T., Toyomura, T., Honjo, K., Wada, Y., and Futai, M. (2001). Four subunit *a* isoforms of *Caenorhabditis elegans* vacuolar H^+-ATPase. J. Biol. Chem. *276*, 3309–33085.

Pohl, A., Devaux, P. F., and Herrmann, A. (2005). Function of prokaryotic and eukaryotic ABC proteins in lipid transport. Biochim. Biophys. Acta *1733*, 29–52.

Pujol, N., Bonnerot, C., Ewbank, J. J., Kohara, Y., and Thierry-Mieg, D. (2001). The *Caenorhabditis elegans unc-32* gene encodes alternative forms of a vacuolar ATPase *a* subunit. J. Biol. Chem. *276*, 11913–11921.

Rajagopal, A., and Simon, S. M. (2003). Subcellular localization and activity of multidrug resistance proteins. Mol. Biol. Cell *14*, 3389–3399.

Raposo, G., and Marks, M. S. (2002). The dark side of lysosome-related organelles: Specialization of the endocytic pathway for melanosome biogenesis. Traffic *3*, 237–248.

Roudier, N., Lefebvre, C., and Legouis, R. (2005). CeVPS-27 is an endosomal protein required for the molting and the endocytic trafficking of the low-density lipoprotein receptor-related protein 1 in *Caenorhabditis elegans*. Traffic *6*, 695–705.

Schneider, E., and Hunke, S. (1998). ATP-binding-cassette (ABC) transport systems: functional and structural aspects of the ATP-hydrolyzing subunits/domains. FEMS Microbiol. Rev. *22*, 1–20.

Sheps, J. A., Ralph, S., Zhao, Z., Baillie, D. L., and Ling, V. (2004). The ABC transporter gene family of *Caenorhabditis elegans* has implications for the evolutionary dynamics of multidrug resistance in eukaryotes. Genome Biol. *5*, R15.

Shulenin, S., Nogee, L. M., Annilo, T., Wert, S. E., Whitsett, J. A., and Dean, M. (2004). ABCA3 gene mutations in newborns with fatal surfactant deficiency. N. Engl. J. Med. *350*, 1296–1303.

Simmer, F., Tijsterman, M., Parrish, S., Koushika, S. P., Nonet, M. L., Fire, A., Ahringer, J., and Plasterk, R. H. (2002). Loss of the putative RNA-directed RNA polymerase RRF-3 makes *C. elegans* hypersensitive to RNAi. Curr. Biol. *12*, 1317–1319.

Spritz, R. A. (1999). Multi-organellar disorders of pigmentation: intracellular traffic jams in mammals, flies and yeast. Trends Genet. *15*, 337–340.

Stinchcombe, J., Bossi, G., and Griffiths, G. M. (2004). Linking albinism and immunity: the secrets of secretory lysosomes. Science *305*, 55–59.

Sulston, J. E., Schierenberg, E., White, J. G., and Thomson, J. N. (1983). The embryonic cell lineage of the nematode *Caenorhabditis elegans*. Dev. Biol. *100*, 64–119.

Treusch, S., Knuth, S., Slaugenhaupt, S. A., Goldin, E., Grant, B. D., and Fares, H. (2004). *Caenorhabditis elegans* functional orthologue of human protein h-mucolipin-1 is required for lysosome biogenesis. Proc. Natl. Acad. Sci. USA *13*, 4483–4488.

Urbatsch, I. L., Beaudet, L., Carrier, I., and Gros, P. (1998). Mutations in either nucleotide-binding site of P-glycoprotein (Mdr3) prevent vanadate trapping of nucleotide at both sites. Biochemistry *37*, 4592–4602.

van Meer, G., Halter, D., Sprong, H., Somerharju, P., and Egmond, M. R. (2006). ABC lipid transporters: extruders, flippases, or flopless activators? FEBS Lett. *580*, 1171–1177.

Weaver, T. E., Na, C. L., and Stahlman, M. (2002). Biogenesis of lamellar bodies, lysosome-related organelles involved in storage and secretion of pulmonary surfactant. Semin. Cell Dev. Biol. *13*, 263–270.

Wei, M. L. (2006). Hermansky-Pudlak syndrome: a disease of protein trafficking and organelle function. Pigment Cell Res. *19*, 19–42.

Welte, M. A., Cermelli, S., Griner, J., Viera, A., Guo, Y., Kim, D. H., Gindhart, J. G., and Gross, S. P. (2005). Regulation of lipid-droplet transport by the perilipin homolog LSD2. Curr. Biol. *15*, 1266–1275.

Wicky, S., Schwarz, H., and Singer-Kruger, B. (2004). Molecular interactions of yeast Neo1p, an essential member of the Drs2 family of aminophospholipid translocases, and its role in membrane trafficking within the endomembrane system. Mol. Cell. Biol. *24*, 7402–7418.

Yamano, G., Funahashi, H., Kawanami, O., Zhao, L. X., Ban, N., Uchida, Y., Morohoshi, T., Ogawa, J., Shioda, S., and Inagaki, N. (2001). ABCA3 is a lamellar body membrane protein in human lung alveolar type II cells. FEBS Lett. *508*, 221–225.

Yang, F. *et al.* (2006). An ARC/Mediator subunit required for SREBP control of cholesterol and lipid homeostasis. Nature *442*, 700–704.

Zha, X., Genest, J., Jr., and McPherson, R. (2001). Endocytosis is enhanced in Tangier fibroblasts: possible role of ATP-binding cassette protein A1 in endosomal vesicular transport. J. Biol. Chem. *276*, 39476–39483.

Zhang, F., Zhang, W., Liu, L., Fisher, C. L., Hui, D., Childs, S., Dorovini-Zis, K., and Ling, V. (2000). Characterization of ABCB9, an ATP binding cassette protein associated with lysosomes. J. Biol. Chem. *275*, 23287–23294.

Zhang, Y., Grant, B., and Hirsh, D. (2001). RME-8, a conserved J-domain protein, is required for endocytosis in *Caenorhabditis elegans*. Mol. Biol. Cell *12*, 2011–2021.

Zhao, C., Tampe, R., and Abele, R. (2006). TAP and TAP-like—Brothers in arms? Naunyn Schmiedebergs Arch. Pharmacol. *372*, 444–450.

Zhao, Z., Sheps, J. A., Ling, V., Fang, L. L., and Baillie, D. L. (2004). Expression analysis of ABC transporters reveals differential functions of tandemly duplicated genes in *Caenorhabditis elegans*. J. Mol. Biol. *344*, 409–417.

Zhou, C., Zhao, L., Inagaki, N., Guan, J., Nakajo, S., Hirabayashi, T., Kikuyama, S., and Shioda, S. (2001). Atp-binding cassette transporter ABC2/ABCA2 in the rat brain: a novel mammalian lysosome-associated membrane protein and a specific marker for oligodendrocytes but not for myelin sheaths. J. Neurosci. *21*, 849–857.